01 Apr 2017

Studies of Hypervelocity Impact Phenomena As Applied to the Protection of Spacecraft Operating in the MMOD Environment

William P. Schonberg
Missouri University of Science and Technology, wschon@mst.edu

Recommended Citation

W. P. Schonberg, "Studies of Hypervelocity Impact Phenomena As Applied to the Protection of Spacecraft Operating in the MMOD Environment," *Proceedings of the 14th Hypervelocity Impact Symposium (2017, Canterbury, UK)*, vol. 204, pp. 4-42, Elsevier, Apr 2017.
The definitive version is available at https://doi.org/10.1016/j.proeng.2017.09.723

Available online at www.sciencedirect.com

ScienceDirect

Procedia Engineering 204 (2017) 4–42

Procedia Engineering

www.elsevier.com/locate/procedia

14th Hypervelocity Impact Symposium 2017, HVIS2017, 24-28 April 2017, Canterbury, Kent, UK

Studies of hypervelocity impact phenomena as applied to the protection of spacecraft operating in the MMOD environment

William P. Schonberg[a]*

[a]*Civil, Architectural, and Environmental Engineering Department, Missouri University of Science and Technology, Rolla, MO 65409*

Abstract

In keeping with the tradition of the Hypervelocity Impact Society, this paper is a written version of the keynote address I presented at the start of 2015 Hypervelocity Impact Symposium as the recipient of the Society's Distinguished Scientist Award. It covers the highlights of my nearly 30 year career working in the area of hypervelocity impact phenomenology, mainly as it is applied to the protection of humans and spacecraft that work an operate in the micrometeoroid and orbital debris (MMOD) environment.

Peer-review under responsibility of the scientific committee of the 14th Hypervelocity Impact Symposium 2017.

Keywords: Spacecraft protection, MMOD, hypervelocity impact

1. Introduction

I am deeply grateful to the Hypervelocity Impact Society, its Awards Committee, and the Board of Directors for selecting to receive the Society's Distinguished Scientist Award at the 2015 Hypervelocity Impact Symposium (HVIS2015). I am humbled when I read the list of the names of previous award recipients, and honored to be included in this distinguished group.

This paper is a written version of the keynote address I presented at the start of HVIS2015. In keeping with tradition, it covers the highlights of my nearly 30 year career working in the area of hypervelocity impact phenomenology, mainly as it is applied to the protection of humans and spacecraft that work an operate in the micrometeoroid and orbital debris (MMOD) environment. Over these past 30 or so years I have been fortunate enough

* Corresponding author. Tel.: +1-573-341-4787.
E-mail address: wschon@mst.edu

1877-7058
Peer-review under responsibility of the scientific committee of the 14th Hypervelocity Impact Symposium 2017.
10.1016/j.proeng.2017.09.723

to work with many talented and gifted graduate students, scientists, engineers, analysts, and modelers, and it is only thanks to their keen insights and assistance that I have been able to accomplish what I have. Special acknowledgements are due, however, to the following individuals:

- Roy Taylor and Miria Finckenor (formerly and currently at the NASA Marshall Space Flight Center, respectively), who gave my career the jump-start it needed when I was a new Assistant Professor at the University of Alabama in Huntsville;
- Joel Williamsen (formerly at the NASA Marshall Space Flight Center and currently with the Institute for Defense Analyses), who has had the burden of working with me for many of these past 30 years on a variety of topics related to space debris;
- Dave Jerome (formerly at Eglin Air Force Base), who introduced me to DoD aspects of hypervelocity impact phenomenologies and studies;
- Klaus Thoma, Frank Schafer, and Robin Putzar (currently at the Ernst Mach Institute), who were kind enough to welcome me to the Fraunhofer Ernst Mach Institute for 7 months as a Humboldt Research Awardee and to give me a much-needed break from my academic administration duties;
- Steve Scott and Mike Squire (currently at the NASA Engineering Safety Center), who have asked me to serve on several NESC Technical Committees, thereby broadening my appreciation of the needs of NASA and its contractors when dealing with the problem of space debris;
- Martin Ratliff (currently at the NASA Jet Propulsion Laboratory), who introduced me to the world of robotic spacecraft and who keeps reminding me that robotic spacecraft have different needs and requirements that human rated spacecraft; and,
- Charlie Anderson, Lalit Chhabildas, and everyone else with whom I have had the pleasure of working as a member of the Hypervelocity Impact Society and who also served as my mentors over the span of my career.

In looking back, it is apparent that the work that I have done has always been about increasing the safety of human space operations. Specifically, whether through data analysis and empirical model development or through modelling efforts that led to suggested possible modifications to ‘standard’ ballistic limit equations for thin multi-wall systems, the primary focus of the work has always been to gain a deeper understanding of the phenomenology involved in high speed impacts so that we can better protect our astronauts and our spacecraft against the hazards and risks posed by MMOD impacts. My career thus far can be thought of as having three phases:

- The early years, as a newly minted Assistant Professor at the UAH, when I spent a lot of time analyzing and making sense of the reams of data that were generated at NASA/MSFC under the Phase B and C/D test programs that supported the development the international space station,
- The middle years, when I ventured to develop analytical models of the various phenomena that occur during a hypervelocity impact, and
- Recent years, when I have be lucky enough to a work on a much wider variety of problems, as well as serving on several NRC/NAE and NESC technical committees.

These phases overlap, of course, and the activities and knowledge gained in one supported the activities and exercises in the other. However, another common thread throughout my work is that I have tended to work in areas or on topics were just outside the more mainstream activities related to high speed impact testing and spacecraft protection. For example, while the majority of the analysis was being performed on normal impact test data obtained using spherical aluminum projectiles, I was intrigued by and directed my energies towards the study of oblique impacts, non-spherical, and non-aluminum projectiles. These activities naturally gave rise to studies on the kind of hole (not simply whether or not there was a hole) in a pressure wall, what happens within a module following a penetrating impact, and characterizing ricochet debris, among others.

In the next few sections I will attempt to summarize the more salient points that have come out of these various studies. In order to understand the context of my work, it is important to first lay out just what exactly constituted the mainstream of testing and analysis work in the area of hypervelocity impact and spacecraft protection in the time period beginning with the late 1980s. It is my hope that future generations of rocket scientists will be able to continue and expand upon these studies as we continue to unravel all the wonder and mysteries associated with these highly energetic phenomena.

2. Setting the stage

The near-earth space environment, where most satellites, the Shuttle, and the International Space Station orbit the earth, is cluttered with naturally occurring micrometeoroids and pieces of man-made orbital debris. This orbital debris ranges in size from microscopic solid propellant particles to spent rocket boosters still in earth orbit. All earth-orbiting spacecraft are therefore susceptible to impacts by these pieces of orbital debris. Although orbital debris ceases to become a threat for interplanetary spacecraft once they leave the confines of earth orbit, they remain susceptible to impacts by meteoroids and other "natural debris."

Orbital debris and meteoroid impacts can occur at extremely high speeds and can damage flight- and mission-critical systems. This can, in turn, lead to spacecraft failure and possibly loss of life. As mission time increases, the probability that such an impact can occur also increases. Therefore, the design of all spacecraft must take into account the possibility of such impacts and their effects on the spacecraft and on all of its exposed system components. For this reason, extensive studies have been performed that are devoted to investigating and assessing these threats, as well as protecting spacecraft through a variety of shielding techniques. To prevent mission failure and/or loss of life, protection against damage by micro-meteoroid and orbital debris (MMOD) particles is typically included in the design of a spacecraft in the form of a hypervelocity impact shield.

Traditional damage-resistant wall design for spacecraft operating in the MMOD environment consists of a 'bumper' wall that is placed at a small distance away from the main or inner wall of the spacecraft component. This concept was first proposed in the 1940s and is referred to as the "Whipple Shield" [1]. It has been studied extensively in the last four decades as a means of reducing the perforation threat of hypervelocity projectiles. A sketch of a typical dual-wall Whipple Shield is shown in Figure 1 (where a multi-layer thermal insulation blanket is shown to occupy a position between the protective bumper and the main inner wall of the spacecraft). Such a dual-wall configuration had been repeatedly shown to provide significant increases in protection against perforation by relatively small high-speed projectiles over an equivalent single-wall structure.

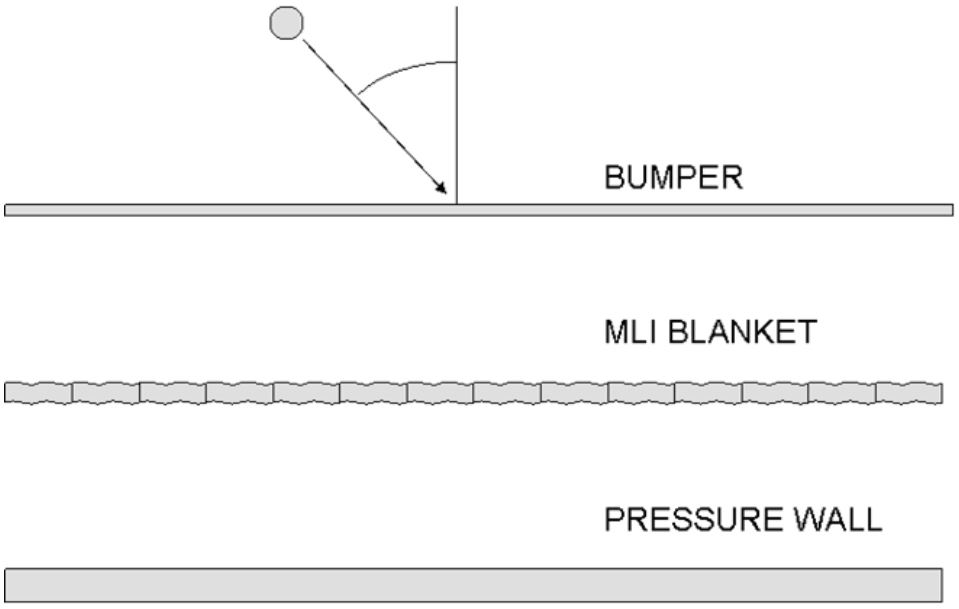

Figure 1. Illustration of a typical dual-wall Whipple Shield

The bumper protects the spacecraft component by disintegrating the impacting particle to create one or more diffuse debris clouds that travel towards and eventually impact the spacecraft element. However, the impacts of these debris clouds impart a significantly lower impulsive loading to the inner wall than would an intact projectile. The area over which this impulsive loading is distributed is governed by the manner in which the projectile and bumper fragment, melt, or vaporize, and by the spacing between the bumper and the inner wall.

Occasionally, the impact of the debris clouds could result in rarefaction stresses near the rear surface of the inner wall that exceed the dynamic tensile fracture strength of the inner wall material. In these cases, spall fragments are ejected further 'inward' at high velocities from the rear side of the inner wall. These high speed particles could themselves inflict damage in internal spacecraft components, such as e-boxes, radiator lines, and cables.

The performance of a hypervelocity impact shield is typically characterized by its ballistic limit equation (BLE), which defines the threshold particle size that causes perforation of, or detached spall from, the inner wall of the multi-wall system as a function of velocity, impact angle, particle density, shield and inner wall thicknesses and particle shape. These BLEs are typically drawn as lines of demarcation between regions of inner-wall perforation and no perforation (P/NP) in two-dimensional projectile diameter-impact velocity space and when graphically represented, are often referred to, in this form, as ballistic limit curves (BLCs).

The high-speed impact testing that provides data for the development of these BLEs and their BLCs typically use spherical projectiles fired in light gas guns at impact velocities between 3 and 7 km/s. These data are then fitted with scaled single-wall equations below approx. 3 km/s, and with theoretical momentum and/or energy based penetration relationships above approx. 7 km/s to obtain three-part BLCs that cover the full range of impact velocity, that is, from approx. 0.5 to 16 km/s for debris, and up to several tens of km/s for meteoroids. The transitional velocity region (from approx. 3 to approx. 7 km/s for normal impacts) takes the form of a linear interpolation between the low and high velocity regions.

Figure 2 below shows generic ballistic limit curves for a dual-wall and an equal-weight single-wall structural system.

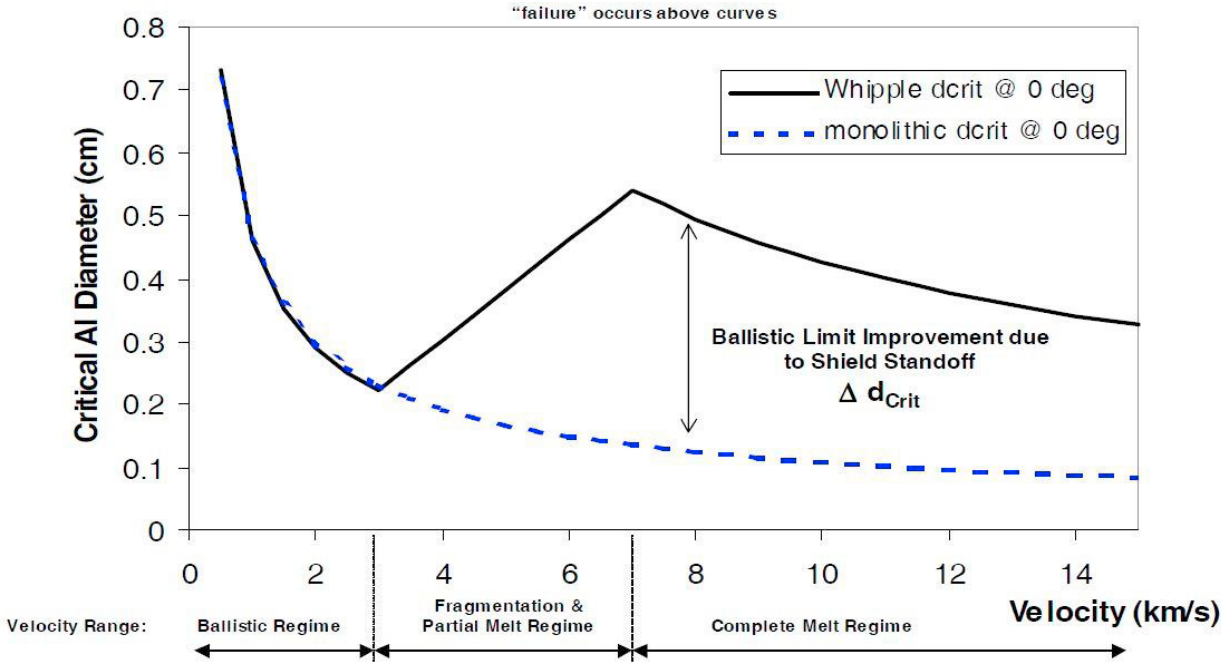

Figure 2. Generic dual-wall and single-wall ballistic limit curves for aluminum-on-aluminum impacts

In Figure 2, the single-wall BLE is seen to be a monotonically decreasing function as impact velocity is increased, while the dual-wall BLE displays the traditional, well-known "bucket" shape of the three-part BLEs that have been developed for such configurations. This shape of the dual-wall BLE is a direct result of the phenomenological changes in response that occur at impact velocities that result in (nearly) complete projectile fragmentation (near 3 km/s for aluminum-on-aluminum impacts) and complete projectile melt (near 7 km/s for aluminum-on-aluminum impacts). The space between the single- and dual-wall equations is a measure of the increase in protection provided by dual-wall systems over that provided by equal-weight single-wall configurations.

Reference [2] presents a history of the development of these types of BLEs. Up through the late 1980s, BLEs such as those shown in Figure 2 were typically derived from tests under the following conditions:

1. normal impact;
2. spherical aluminum projectiles;
3. flat unstressed aluminum plates; and,
4. light-weight thermal insulation blankets (if included at all).

In the early 1990s, as the international space station became a reality, the sophistication of testing programs and analysis capabilities improved greatly. As a result, these limited test parameters and configurations evolved to include non-normal (or oblique) impacts of non-spherical, non-aluminum projectiles impacting targets more representative of spacecraft components (e.g. tiles, e-boxes, wire harnesses, or dual-wall systems with more complex intermediate blankets, etc). It was at this exciting time that I entered the arena of space debris protection system analysis and design, and was confronted with a wealth of new information that needed to be studied and analyzed.

3. Oblique impacts

In the majority of early investigations of hypervelocity impact, the trajectories of the projectiles were normal to the surfaces of the impacted test specimens. However, it is evident that most meteoroid or space debris impacts will not occur normal to the surfaces of a spacecraft. Unfortunately, information on oblique hypervelocity impact was relatively scarce in the 1980s, so was difficult to assess the severity of such impacts on a candidate spacecraft wall structural system. Furthermore, studies of oblique impact that had been performed previously typically did not discuss the possibility of damage to external systems due to ricochet debris particles. To increase the understanding of phenomena associated with oblique hypervelocity impact, light gas gun tests conducted at NASA in the late 1980s and early 1990s began to include more non-normal impact firings to generate (and to subsequently analyze) oblique hypervelocity impact test data.

Figure 3 shows a sketch of the dual-wall test configuration (without any intervening MLI), while Figure 4 shows the formation of penetration and ricochet debris clouds in a 45-deg impact [3].

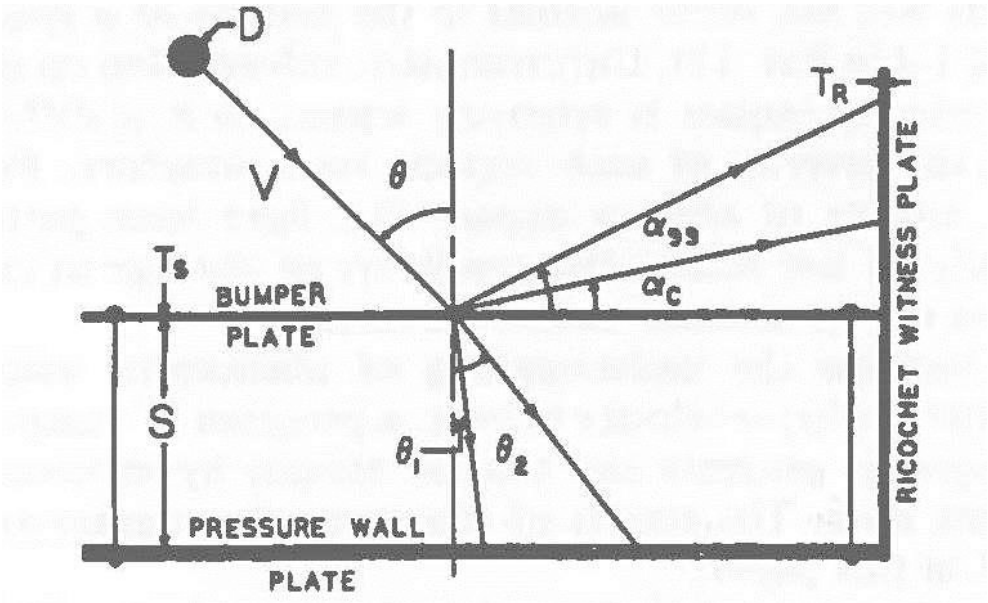

Figure 3. Dual-wall test configuration

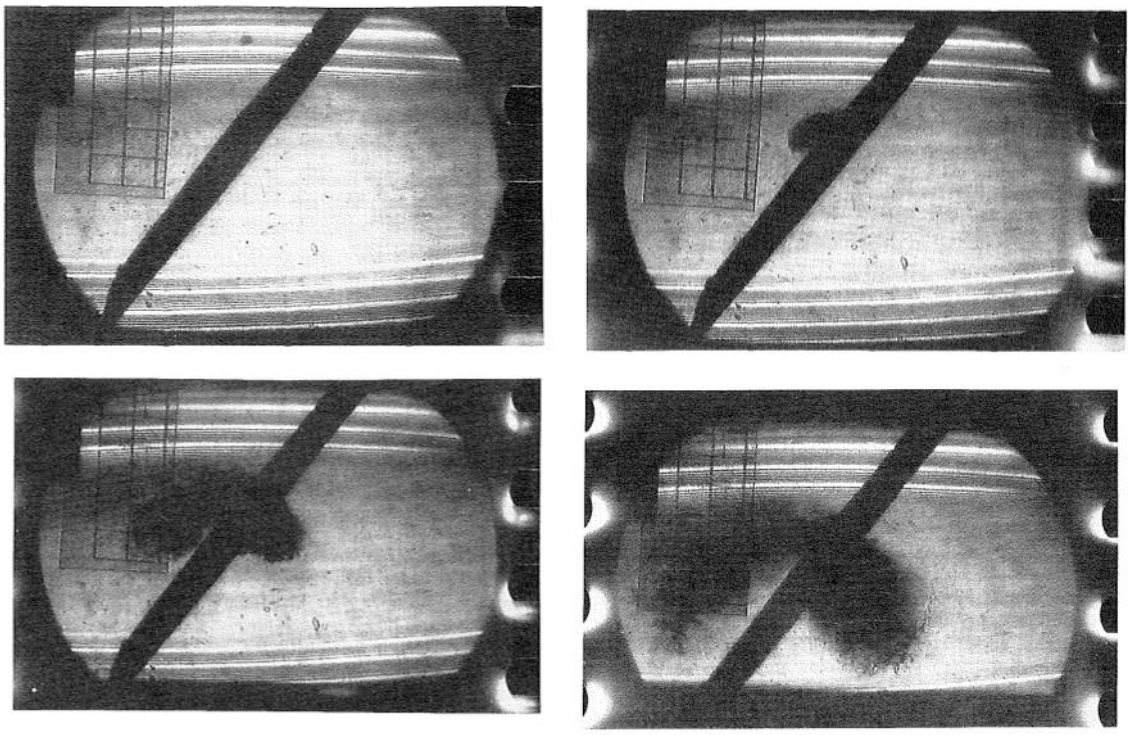

Figure 4. Formation of ricochet and penetration debris clouds, v~6 km/s, θ=45-deg, t_s/d_p~3 (from [3])

Figures 5-8 show typical changes in the damage morphology that is sustained by pressure walls as the impact obliquity is increased [4]. The specific tests shown in Figure 5-8 were performed at impact velocities of ~7 km/s using 7.95 mm diameter aluminum projectiles. The bumper, pressure wall, and ricochet witness plates were made of 6061-T6, 2219-T87, and 2219-T6 aluminum, respectively. Their thicknesses were held constant at 1.6, 3.175, and 2.54 mm, respectively. These figures also show the damage sustained by the ricochet witness plates in each of those tests.

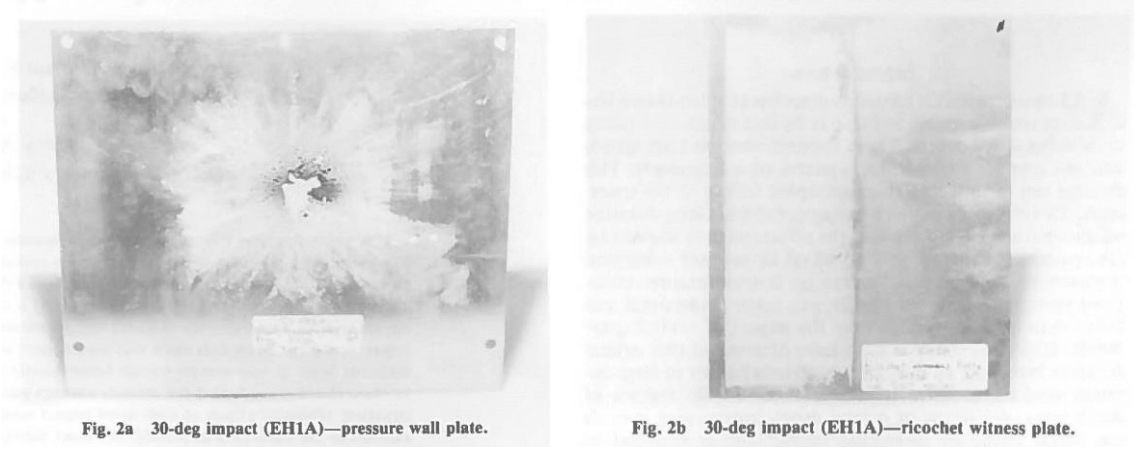

Fig. 2a 30-deg impact (EH1A)—pressure wall plate.

Fig. 2b 30-deg impact (EH1A)—ricochet witness plate.

Figure 5. Damaged pressure wall and ricochet witness plate, 30-deg impact (from [4])

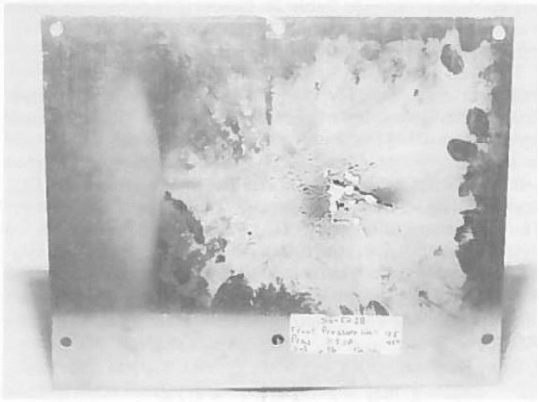

Fig. 3a 45-deg impact (EH1B)—pressure wall plate.

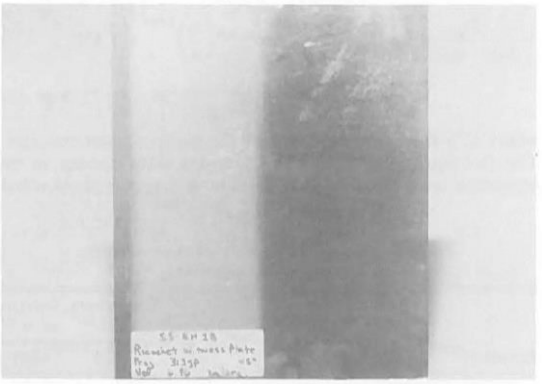

Fig. 3b 45-deg impact (EH1B)—ricochet witness plate.

Figure 6. Damaged pressure wall and ricochet witness plate, 45-deg impact (from [4])

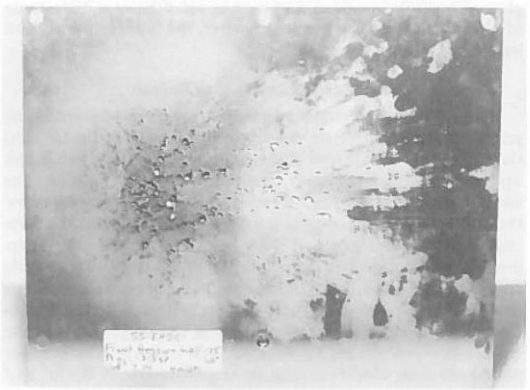

Fig. 4a 60-deg impact (EH1C)—pressure wall plate.

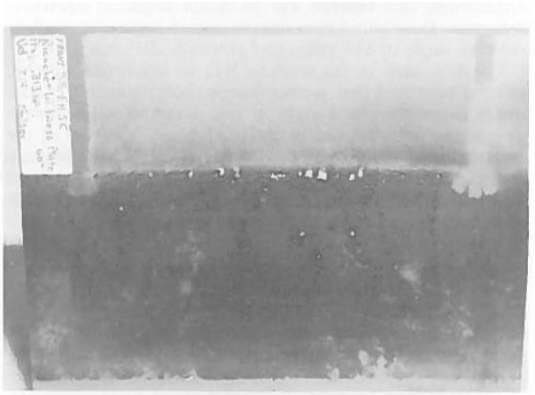

Fig. 4b 60-deg impact (EH1C)—ricochet witness plate.

Figure 7. Damaged pressure wall and ricochet witness plate, 60-deg impact (from [4])

Fig. 5a 75-deg impact (EH1D)—pressure wall plate.

Fig. 5b 75-deg impact (EH1D)—ricochet witness plate.

Figure 8. Damaged pressure wall and ricochet witness plate, 75-deg impact (from [4])

It quickly became evident from these and other follow-on tests that the damage potential of ricochet debris could be quite high, especially for very high obliquity impacts. It was also found in these studies that beyond a certain critical impact angle, the in-line penetrating debris cloud no longer followed close to the original impact trajectory, but rather began to bend back towards the normal between the bumper and the pressure wall. It was also beyond this critical angle that particle damage to the ricochet witness plate became quite substantial. This critical angle was estimated to have a value of 60-deg to 65-deg.

All ricochet debris poses a threat to external spacecraft components that lie in its path. However, the threat could be very significant in the case of highly oblique impacts, which, from Figures 7 and 8, can be surmised to produce debris clouds with relatively large ricocheting particles. An empirical model was developed to characterize the ricochet ejecta particles that would be created by a high speed impact on a typical bumper plate [5]. Specifically, the model developed predicts the spread and trajectory of ricochet debris particles created in a hypervelocity impact as well as the size and velocity of the most damage particle in the ricochet debris cloud.

The table in Figure 9 presents a comparison between the average ricochet debris particle diameters and velocities calculated in a previous experimental study and the average particle velocities and diameters calculated using the empirical model. As can be seen from this figure, the average diameter values predicted by the equations developed in this study compare favorably with those calculated previously. However, the average velocity values predicted by the model are approximately twice the values reported previously.

	d_{avg} (cm)		V_{avg} (km/s)	
θ_p (deg)	Reference [6]	This Study	Reference [6]	This Study
45	0.174	0.121	2.07	4.25
60	0.221	0.204	2.01	4.42
75	0.357	0.348	2.35	4.78
d_p (cm)	Reference [6]	This Study	Reference [6]	This Study
0.475	0.203	0.164	2.17	4.35
0.635	0.258	0.224	2.15	4.49
0.795	0.303	0.285	2.08	4.61

Figure 9. Comparison of average empirical and predicted ricochet particle diameters and velocities (Reference [6] in [5] same as [6] in this paper).

4. Use of composite materials

As mentioned previously, the traditional approach to mitigating the damage that would be caused by high-speed on-orbit MMOD impacts consists of placing one or more “bumper” shields small distances away from the primary load-bearing “inner wall” of the spacecraft. Behind the inner wall of such a multi-wall system, as in the case of the International Space Station, for example, are located the equipment racks, crew quarters, science experiment hardware, etc. With the advent of many new high-strength composite materials and their proliferation in aerospace applications, it quickly became evident that it was necessary to evaluate their potential for use as part of a multi-wall configuration in long-duration space and aerospace structural systems such as the international space station.

Furthermore, most satellites launched into Earth orbit are constructed with honeycomb sandwich panels as their primary structural load bearing elements without a bumper shield because design, cost, and / or mission constraints prevent the inclusion of a protective shield. In these cases, the load-bearing honeycomb sandwich panels (HC/SPs) also serve as the protection systems for the spacecraft components that are located behind them, such as electronics, avionics, fuel cells, pressure vessels, etc. In both cases it is important to know whether or not the impacting particle (or its remnants) will exit the rear of a spacecraft wall system, whether it is a “Whipple-type” multi-wall system or a “single” HC/SP wall.

References [7,8] contain a historical overview of the high-speed impact testing of composite material panels and HC/SPs. Not surprisingly, the extent of the effort to study composite material and composite structural systems such as HC/SP panels has been much more limited than the effort exerted in the study of metallic (mostly aluminum) multi-

wall systems under similar impact conditions. For example, a review of the papers presented at the International Ballistics Symposia (published by the host organization) and the Hypervelocity Impact Symposia (published by Elsevier) allows us to construct the histogram shown in Figure 10. Also shown in Figure 10 is an accounting of papers on this topic appearing in other venues and journals. As can be seen in Figure 10, interest in this area of research is increasing, especially since the 1990s.

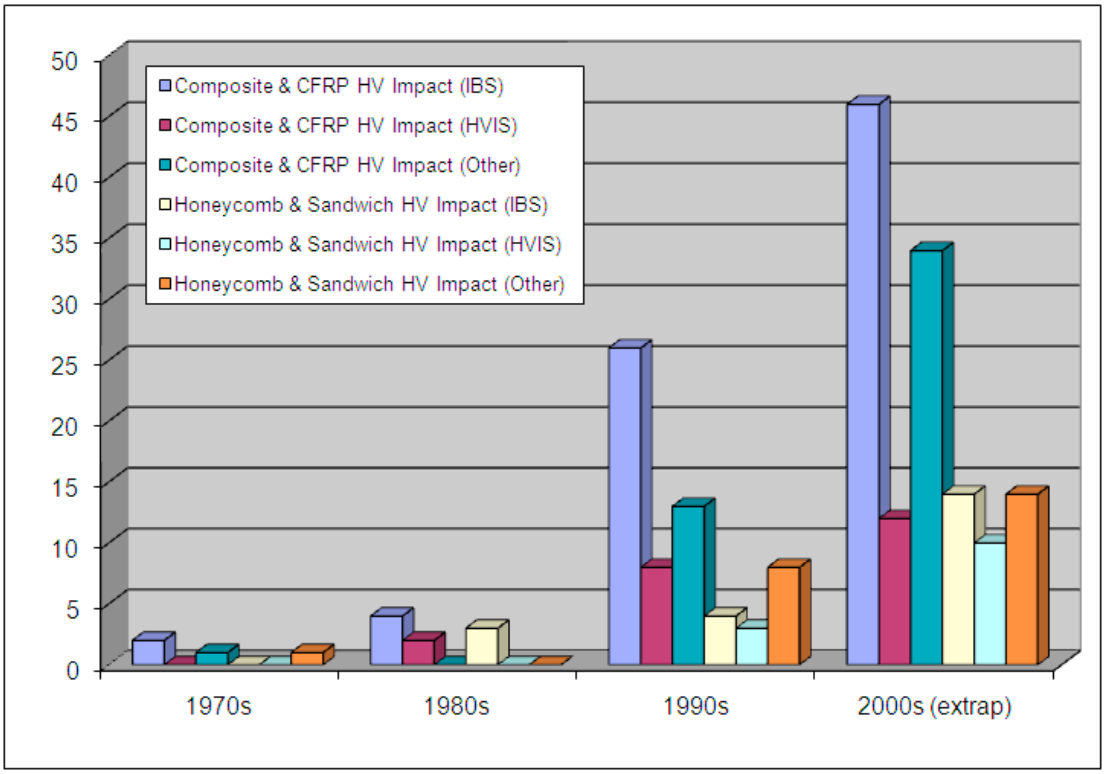

Figure 10. Number of papers on composite and HC/SP HVI

My early work in this area explored changes in the level of protection that would be afforded to a spacecraft if composite materials were used either as bumpers, stuffing, or as pressure walls. More recent work focused on characterizing impact response of HC/SPs under hypervelocity impacts. The following paragraphs summarize the main conclusions reached in these studies. Additional more detailed information on the use of composite materials in multi-wall systems or on the response of HC/SPs under high-speed impact can be found in References [9] and [10], respectively.

4.1. Composite outer bumpers

The response of dual-wall systems with Kevlar and graphite/epoxy (Gr/Ep) outer bumpers was compared against that of equal-weight all-aluminum dual-wall systems in the late 1980s by Schonberg [11]. The aluminum bumpers were more effective in spreading out the debris created by the initial impact on the bumper than were the Kevlar bumpers. Apparently the interaction of the shock waves in the projectile and the Kevlar bumpers prevented complete break-up of the projectiles, which decreased the dispersion of debris cloud fragments, thereby increasing the likelihood of pressure wall perforation. However, the pressure wall damage areas in dual-wall systems with Gr/Ep bumpers more wide-spread than those in equivalent systems with Kevlar bumpers. Pressure wall perforations in Gr/Ep systems consisted of several small holes, not one large hole as in the Kevlar systems. From these results, it was concluded that using a laminated composite as the outer bumper in a dual-wall system does not offer any protection advantage as compared to the protection level provided by an all-aluminum dual-wall system.

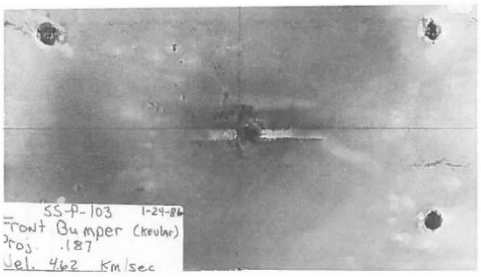

Fig. 2a. Bumper Plate, Front (Test No. 103)

Fig. 3a. Bumper Plate, Front (Test No. P27)

Fig. 2c. Pressure Wall Plate, Front (Test No. 103)

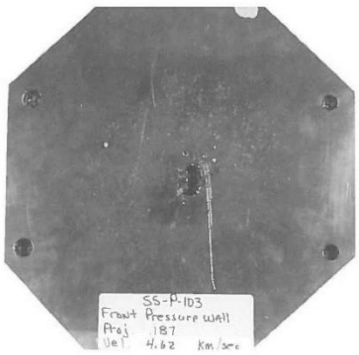

Fig. 3b. Pressure Wall Plate, Front (Test No. P27)

Figure 11a,b. Graphite/epoxy bumper and aluminum pressure wall plate (from [11])

Figure 12a,b. Aluminum bumper and aluminum pressure wall plate (from [11])

Figures 11a,b and 12a,b show the damage sustained by systems with Gr/Ep bumpers and aluminum pressure wall plates and that in corresponding systems with aluminum bumpers and aluminum pressure wall plates under very similar high speed impact conditions. As expected, there is significant peeling of the outer layers in the Gr/Ep bumper, on the front and rear surfaces. The nature of the hole in the pressure wall plate in the test with the Gr/Ep bumper also indicates that the projectile passed through the bumper nearly intact. This is in sharp contrast to the evidence of the pressure wall plate in the test with the aluminum bumper. In this case the diffuse damage area on the pressure wall shows that the projectile was substantially broken up by the aluminum bumper.

These results were supported by Christiansen [12], who performed an in-depth study in the early 1980s to evaluate the effectiveness of metallic, composite, and ceramic materials as MOD shields. Christiansen found that while Gr/Ep alone did not shield as well as did aluminum, it had some potential to enhance MOD protection levels when used as the second bumper in a double-bumper system with an aluminum outer bumper. The use of composite materials as inner bumpers is discussed in the next section.

4.2. Composite inner bumpers

The response of triple-wall systems with Kevlar and Spectra inner bumpers was compared against that of all-metallic triple-wall systems [13]. In nearly all the Kevlar inner bumper tests the Kevlar panels were not perforated, whereas their aluminum counterparts sustained large holes. In the Spectra tests, both the Spectra and aluminum inner bumpers were perforated. However, the pressure walls in the Spectra systems sustained little or no damage, while those in corresponding all-aluminum systems were usually perforated. These results demonstrate that using a composite material as the inner bumper does increase the protection afforded to a spacecraft against damage caused by MMOD impacts.

Figures 13a,b and 14a,b show the damage sustained by systems with Spectra inner bumpers and aluminum pressure wall plates and that in corresponding systems with aluminum inner bumpers and aluminum pressure wall plates under nearly identical impact conditions. The pressure wall in the system with the Spectra inner bumper is barely damaged while that in the all-aluminum system sustained (as is more typical) a much wider area of damage (and in this case even a small perforation).

Fig. 7. Spectra/epoxy intermediate bumper, test no. SPR-12.

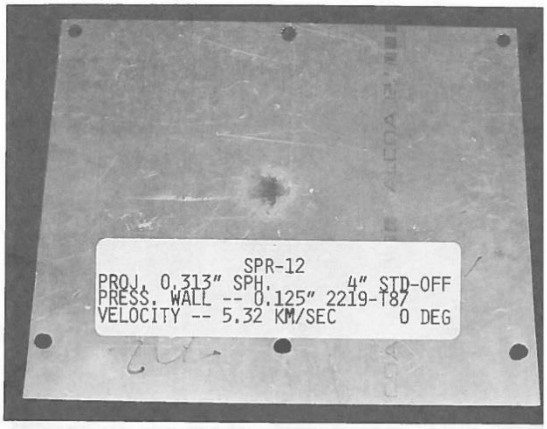

Fig. 8. Aluminum pressure wall plate, test no. SPR-12.

Figure 13a,b. Spectra inner bumper and aluminum pressure wall plate (from [13])

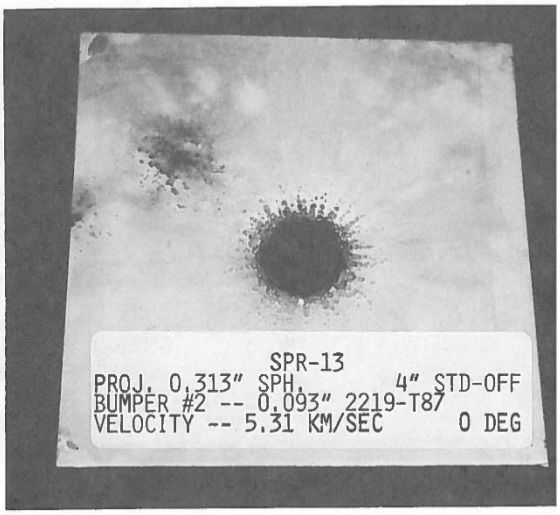

Fig. 9. Aluminum intermediate bumper, test no. SPR-13.

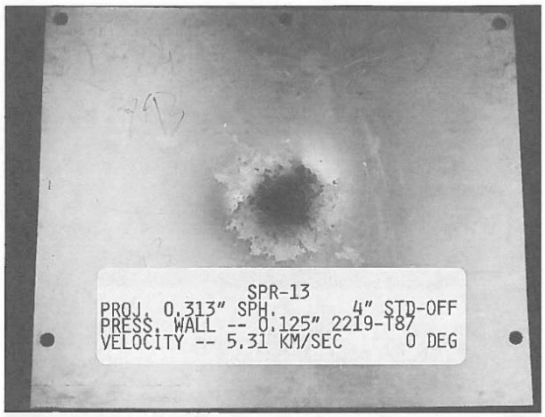

Fig. 10. Aluminum pressure wall plate, test no. SPR-13.

Figure 14a,b. Aluminum inner bumper and pressure wall plate (from [13])

As summarized in Reference [14], the results of the various test programs performed showed that multi-wall systems involving composite material bumpers in combination with aluminum bumpers produced less damaging secondary debris or ejecta, and were

- more efficient in converting the projectile's kinetic energy into internal thermal energy,
- less sensitive to projectile shape, and
- less sensitive to the obliquity of the impacting projectile.

Furthermore, such hybrid systems resulted in less cumulative damage to the pressure wall of the multi-wall system when compared with traditional Whipple-type all-aluminum single-bumper systems [15]. As a result, such systems were found to provide better protection against more hazardous non-spherical projectiles when compared to the protection level offered by all-aluminum systems [16].

4.3. Composite pressure walls

In the mid-1990s, a study was performed to compare the response of dual-wall systems with Graphite/Epoxy (Gr/Ep) pressure walls against that of equal-weight all-aluminum dual-wall systems [17]. The results showed there are several advantages of using Gr/Ep as a pressure wall material: (1) it eliminates severe cracking and petalling sustained by aluminum walls in systems impacted by large projectiles; (2) its ballistic performance is superior to that of aluminum for impact velocities above 5.5 km/s; and (3) patching a hole in a perforated Gr/Ep panel, even if it were larger than in an aluminum panel, would be relatively easy since the Gr/Ep remains non-deformed and the patch can be, e.g., adhesively bonded. Repairing a perforated aluminum wall would be a more difficult procedure since the aluminum would likely be cracked and petalled. On-orbit repair of perforated aluminum panels would therefore require cutting and welding tools that are EVA compatible, while the repair of perforated Gr/Ep panels would not.

Table 3. Test-by-test results and comparisons—
graphite/epoxy inner wall systems vs similar-weight aluminum inner wall systems

Test no.	Impact velocity ($km\ s^{-1}$)	Inner wall material	Inner wall hole dimension (cm)	Primary inner wall damage area diameter (cm)	Secondary inner wall damage area diameter (cm)	Inner wall bulge depth (cm)	Rear surface damage area diameter (cm)	Witness plate 1 damage	Witness plate 2 damage
CRW-1	5.68	Graphite/epoxy	np	5.1	13.9	—	12.7 × 53.3	nd	nd
3034C	5.60	2219-T87	2.5 × 3.1†	7.6	11.3	2.0	nd	splash	nd
CRW-2	5.41	Graphite/epoxy	1.8 × 5.2	5.1	13.9	—	12.7 × 53.3	1 dent	nd
3034C	5.60	2219-T87	2.5 × 3.1†	7.6	11.3	2.0	nd	splash	nd
CRW-3	4.70	Graphite/epoxy	1.8 × 3.8	5.1	12.7	—	11.5 × 45.7	1 dent	nd
3034A	4.50	2219-T87	0.3 × 0.9‡	5.1	10.2	1.5	nd	3 craters	nd
CRW-4	3.73	Graphite/epoxy	2.8 × 2.8	5.1	11.5	—	10.2 × 38.1	bulge	nd
3034B	3.63	2219-T87	0.6 × 0.6‖	2.5	10.8	1.2	nd	4 dents	nd

†Three cracks emanating from hole, 3.18, 5.08 and 5.72 cm long.
‡Two cracks emanating from hole, 3.18 and 3.51 cm long.
‖Two cracks emanating from hole, 3.81 and 4.27 cm long.

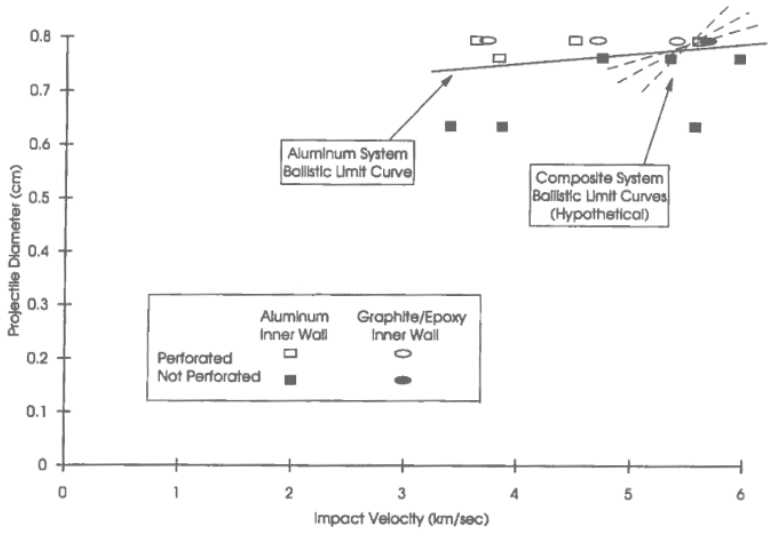

Fig. 2. Performance of dual-wall structures with aluminum and graphite/epoxy inner walls.

Figure 15. Comparison of graphite/epoxy and aluminum pressure walls (table and figure from [17])

Figure 15 shows a summary of the test results for similar systems with Gr/Ep and aluminum pressure wall. As can be seen from this figure, the ballistic resistance of these two systems was similar below approx. 5.5 km/s; above that velocity, there began to be some differences in response.

4.4. Response of HC/SPs

Initial testing of HC/SPs in the 1960s and 1970s produced mixed results and inconsistent predictions regarding the ability of such systems to withstand hypervelocity MMOD impacts. High speed impact testing of HC/SPs experienced a resurgence in the late 1980s and early 1990s when an increasing number of satellites were being designed with HCSPs as the main load-bearing structural elements and subsequently subjected to potential impacts by man-made debris in earth orbit. Test programs performed in support of these satellite design and construction activities considered not just the impact of the HC/SP, but also what would be the effects of penetrating high speed impacts on the satellite systems behind the HC/SP (e.g. fuel pipes, heat pipes, pressure vessels, electronics boxes, harnesses, and batteries).

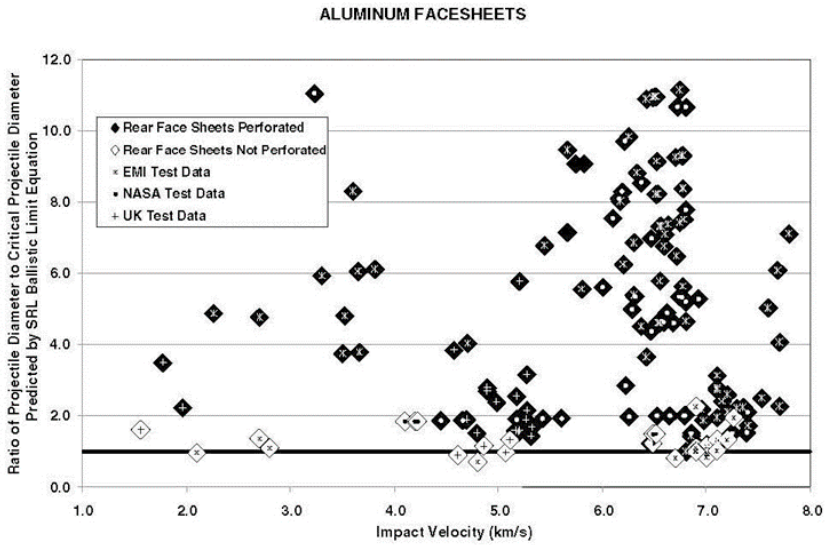

Fig. 4 Prediction of HC SP perforation and nonperforation using the SRL BLEs for aluminum face sheets.

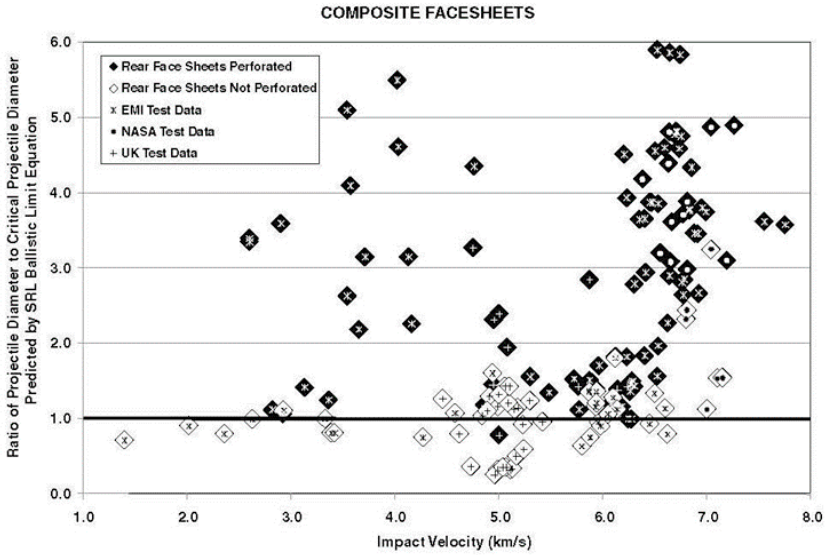

Fig. 5 Prediction of HC/SP perforation and nonperforation using the SRL BLEs for composite face sheets.

Figures 16a,b. Prediction of HC/SP perforations (from [20])

One outcome of these spacecraft component vulnerability studies was a new BLE that could be applied to various structural configurations, including single wall systems, dual-wall systems, multi-wall systems with HC/SPs, batteries, e-boxes, harnesses, etc. [18,19]. To assess how well these BLEs performed in terms of predicting perforation (P) or non-perforation (NP) of HC/SP systems with aluminum and composite face-sheets, an exercise was undertaken to compare the P/NP predictions of the equations in [18] and in [19] against actual P/NP occurrences as found in the data from the experimental investigations discussed in this section [20]. It was found that these BLEs are fairly conservative: they successfully predicted HC/SP perforation in nearly all of the tests that resulted in perforation, while allowing approximately half of the non-perforating tests to be incorrectly labeled as tests with a perforation (see Figures 16a,b for perforation prediction of HC/SPs with aluminum and composite face-sheets, respectively). This indicates the likelihood that use of these BLEs in design applications could result in overly robust shielding hardware.

In addition to knowing whether or not the impacting particle (or its remnants) will exit the rear of the HC/SP, it is equally important to know, if indeed the ballistic limit of the HC/SP has been exceeded, where the debris created in such an impact will land and what internal components it will strike (see Figure 17).

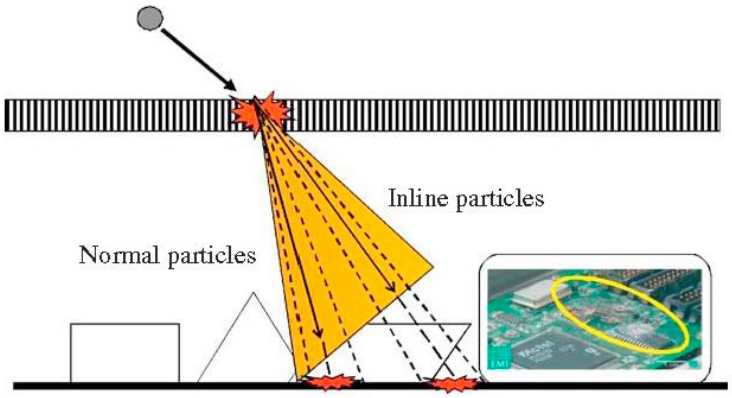

Figure 17. Debris from a perforating impact striking interior spacecraft components

To help address this issue, a system of empirical equations that can be used to predict the trajectories and spread of the debris clouds that exit the rear face-sheet following a high speed perforating impact of a HC/SP was recently developed [21]. The equations developed in this study incorporate the following features:

- presence (or the lack thereof) and composition of a multi-layer thermal insulation (MLI) blanket on the exterior of the HC/SP;
- material composition of the HC/SP face-sheets (either aluminum or a carbon-fiber-reinforced polymer, or CFRP);
- face-sheet thicknesses and overall HC/SP thickness;
- HC core properties (core size, wall thickness, and material);
- the ballistic limit of the HC/SP (see Figure 18), and;
- projectile diameter, material, impact velocity, and trajectory obliquity.

Empirical equations were also developed to predict the dimensions of the holes in the front and rear HC/SP face-sheets. These hole dimension equations can be used to calculate the amount of mass in a debris cloud if the HC/SP is perforated by a high speed impact. The trajectory angles can then be used to determine where this mass will travel and what spacecraft components will be impacted, and the spread angles equations will determine the extent of the footprint made by this mass on any encountered surface. All of this information can then be fed into a risk assessment code to calculate the probability of spacecraft failure under a prescribed set of impact conditions.

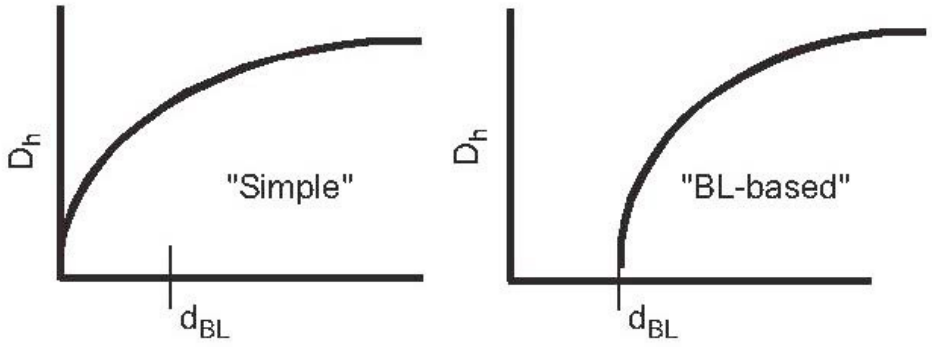

Figure 18. Difference between “simple” and “BL-based” empirical equations

5. Non-spherical projectiles

As a practical matter, most of the BLEs in use have been constructed from impact test databases involving only spherical projectiles. When using spherical projectile, impact orientation is a non-issue. When using cylindrical, chunky, or disk projectile, the orientation of the projectile upon impact on the bumper plays a crucial role in determining the subsequent response of the pressure wall. Figure 19 shows a rather unusual perforation morphology following the (presumed) normal impact of an L/D=1 cylindrical projectile [22].

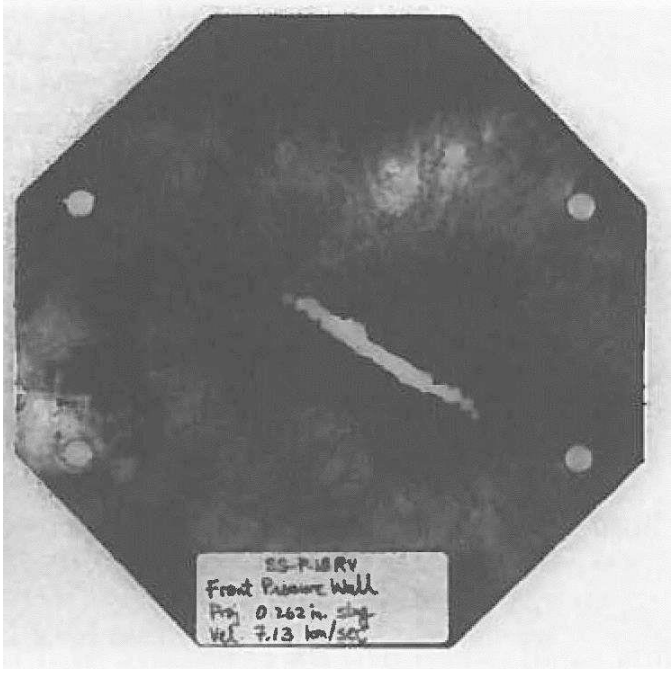

Figure 19. Hole in Pressure Wall Plate of a Dual-Wall System following the Normal Impact of a Cylindrical Projectile.

Morrison [23], Piekutowski [24], and others have shown that non-spherical projectiles can be more damaging than equal mass spherical projectiles under the same impact conditions. In the case of rod-like projectiles, this is mostly due to the incomplete fragmentation of the incoming projectile by the bumper. The intact portion of the projectile is clearly evident in Figure 20, which shows a frame from the numerical simulation of an L/D=2 projectile on a dual-wall system [25].

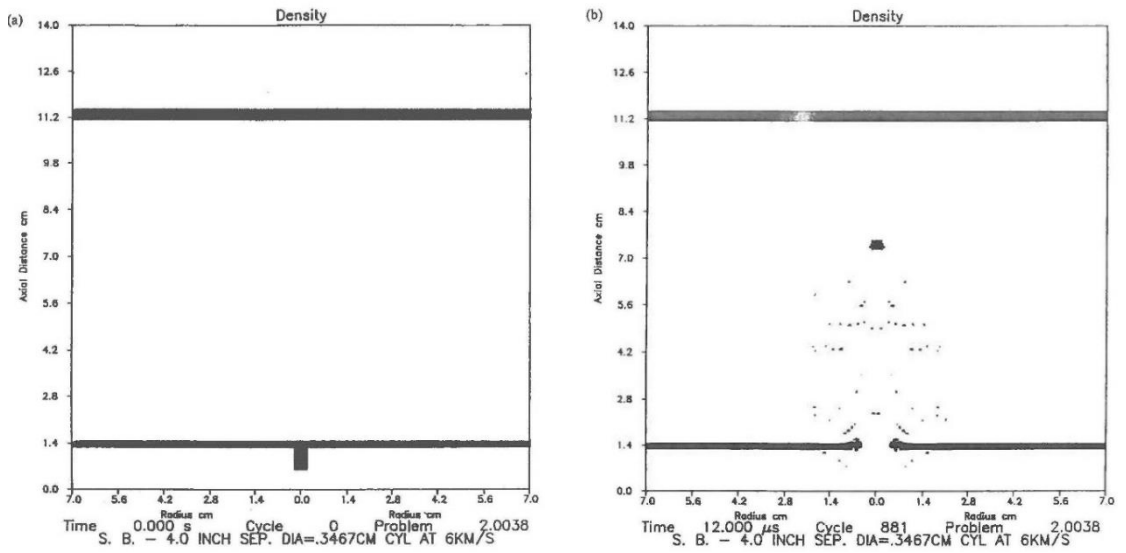

Figure 20a,b. Numerical Simulation of an L/D=2 Cylinder Impacting a Dual-Wall System

Of course, spheres are not expected to be a common shape for orbital debris; rather, orbital debris fragments might be better represented by other regular or irregular solids. A study was performed to develop BLEs and their corresponding curves (BLCs) for a typical dual-wall configuration impacted by a variety of non-spherical projectiles [26]. Figure 21 shows the projectile shapes that were considered in that study. The responses of the dual-wall system to impacts by the projectiles shown in Figure 17 were obtained using the AUTODYN software package.

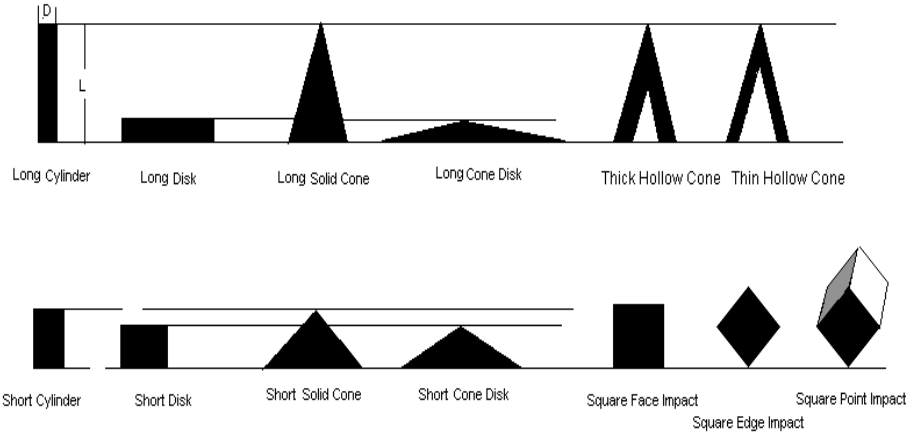

Figure 21. Projectile Shapes Used in BLE Development Study

For each shape, impact simulations were conducted at velocities ranging from 1 to 15 km/s. Projectile mass was increased to a point where the projectile (or ensuing debris cloud) was able to perforate the rear wall. BLCs were then drawn between regions of rear-wall perforation and no-perforation in 2-D projectile mass-impact velocity space. In order to make the various non-spherical projectile BLCs comparable to the spherical projectile-based curves, the non-spherical projectiles mass–impact velocity curves were converted into equivalent spherical diameter–impact velocity curves using an equal mass consideration. Equivalent spherical projectile diameters were calculated by equating the volume of a sphere to the volume of the projectile being considered and then by solving the sphere's diameter. Figure 22 shows the resulting family of BLCs for the non-spherical projectiles considered, as well as for a sphere.

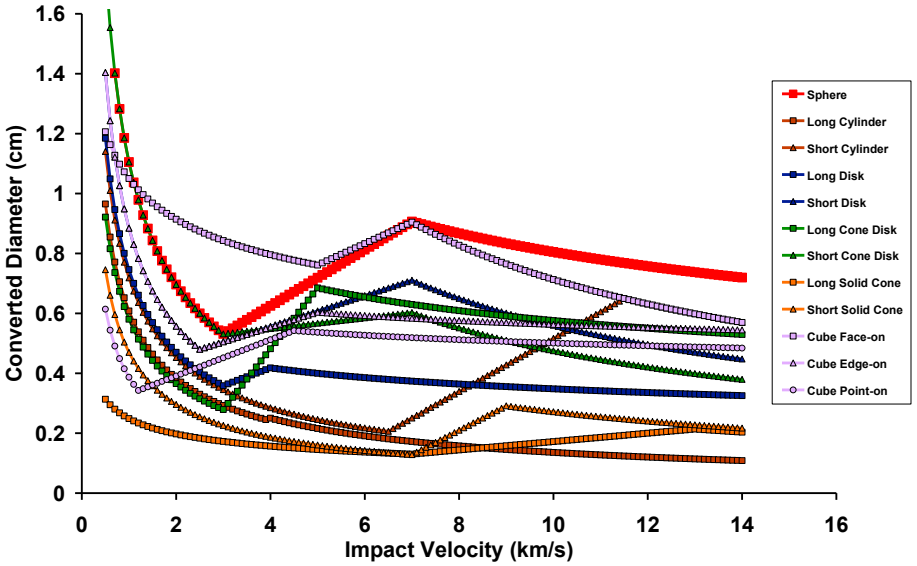

Figure 22. Numerically-based Ballistic Limit Curves for Non-Spherical Projectiles

As expected, the short or chunky projectiles (sphere and face-on cube impact) had the least perforating ability, while those of the longest solid projectiles (cylinder and cone) were the highest. The implication of these results is that if a spacecraft wall system were designed using spherical projectile-based BLCs, the design could be highly non-conservative and possibly unsafe.

It is also important to note that that the BLCs in Figure 22 were drawn in terms of equivalent spherical projectile diameter as a function of impact velocity. However, in order to be useful for spacecraft design, BLCs need to be presented in units that are consistent with environment flux models used in that design process. Current orbital debris re-entry models use a single one-dimensional characteristic length that is effectively a radar cross-section (RCS) diameter. BLCs that are presented in a format that employs a characteristic length instead of an equivalent spherical diameter are likely to be more consistent with orbital debris environment predictions, and should find greater utility in spacecraft risk assessment and design.

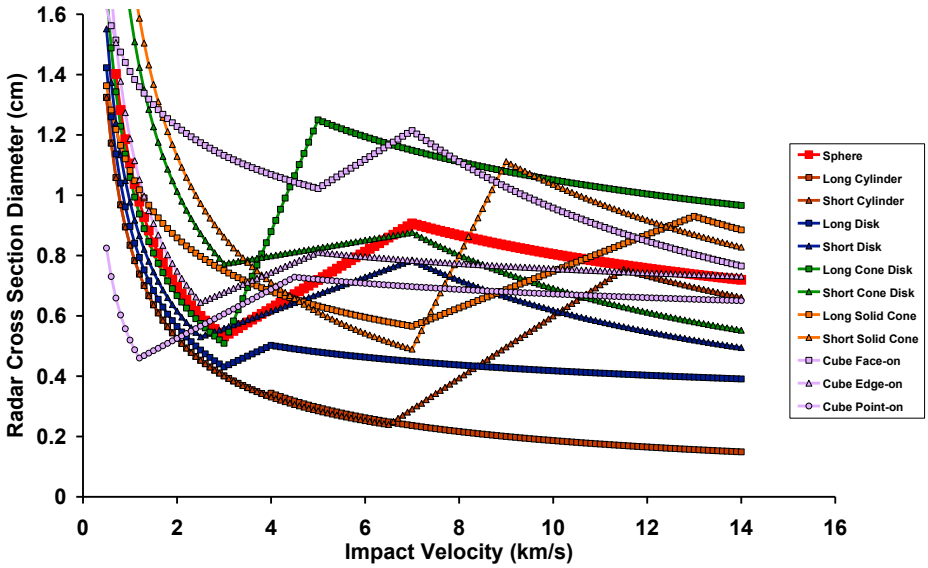

Figure 23. Non-Spherical Projectile BLCs Re-Cast using RCS

In a follow-on study [27], the BLCs in Figure 22 were re-cast using an RCS diameter as the characteristic length. The recast BLCs were found to be more tightly grouped, and were not as spread out as they were when simply plotted using equivalent spherical projectile diameter (see Figure 23). As a result, the effect of projectile shape on penetrating ability was shown to be somewhat reduced when using characteristic length as opposed to equivalent mass for comparison purposes.

One of the major conclusions of this study was that, at least from an RCS characteristic length perspective, the spherical projectile is not necessarily the least conservative projectile shape on which to base or develop a BLC for a multi-wall system. This was in stark contrast with the then-prevailing wisdom which presumed that spherical projectiles are the least damaging of all shapes.

The need for a more realistic projectile size and shape in risk assessments was revisited in two recent studies on the susceptibility of dual-wall structures [28] and the Orion Crew Exploration Vehicle (CEV) to MMOD impacts [29]. For the purposes of performing penetration risk analyses, NASA currently assumes that the shape of the impacting orbital debris particle is a sphere, with a diameter equal to the particle characteristic length. A number of different ground-based experiments have generated mass distributions for typical orbital debris fragments that could be expected to impact spacecraft. These tests have also shown that the much smaller fragments tend to be chunkier or more 'cube-like', while the larger fragments are more flake-like, and being to resemble potato-chips in shape.

The mass distribution from such tests are plotted versus their measured characteristic length (LC) in Figures 24a-d. Also plotted in each figure are the mass values for spheres having the characteristics lengths as diameters (the red lines). It is apparent in these figures that the masses of spheres with diameters equal to LC values above the "crossing points" are higher than the masses of the corresponding actual fragments at those characteristic lengths.

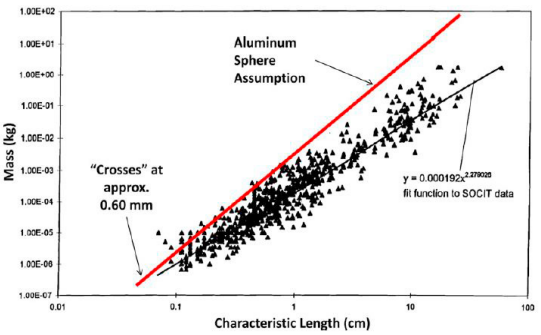

Fig. 5. Comparing mass of satellite fragments to aluminum spheres, Original SOCIT data (Reynolds et al., 1998).

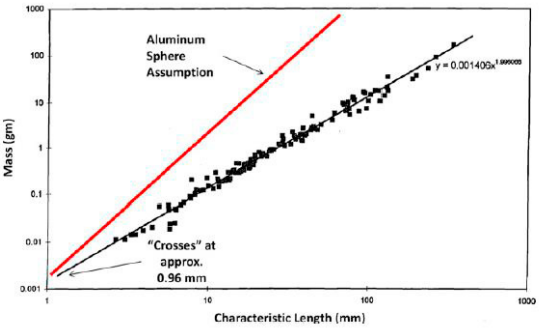

Fig. 7. Comparing mass of upper stage fragments to aluminum spheres, ESOC data (Fucke et al., 1993).

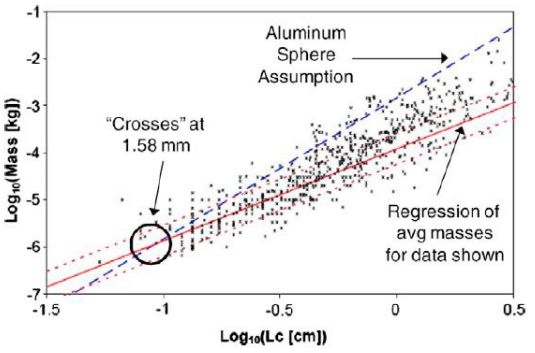

Fig. 6. Comparing mass of satellite fragments to aluminum spheres, revised SOCIT data (Matney, 2008).

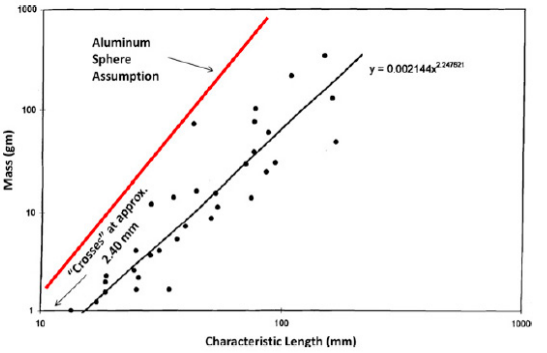

Fig. 8. Comparing mass of RCS fragments to aluminum spheres (Reynolds et al., 1998).

Figure 24a-d. Comparison of Satellite Fragment Masses to Aluminum Sphere Equivalents (from [29])

As such, when LC exceeds the "crossing point" value, the realistic (i.e. non-spherical) debris fragments are less penetrating than currently assumed, an assumption which in turn currently leads to an over-prediction of risk. Offsetting this to some degree, however, is the simplifying presumption of shape – as seen before, for a given mass,

non-spherical particle shapes can be more penetrating than a sphere. An actual orbital debris fragment, therefore, can be either more or less penetrating than that being estimated by the solid sphere of the same 'size' (i.e., by taking characteristic length equal to spherical diameter), depending on which of these two effects dominates. The fragment will be less penetrating because of the smaller mass, but may be more penetrating because of the irregular shape.

This study also showed that, after taking all these competing issues into considerations, continuing to use aluminum spheres in spacecraft risk assessments could result in assessed risk values that might be higher by a factor of 2 than those obtained if more realistic projectile shapes were used. In such a case, there could be an over-design of a spacecraft's MMOD protection systems, and the spacecraft would be heavier than needed, cost more to construct than needed, and cost more to put into orbit than needed. This study demonstrated the need to incorporate effects of mass and shape in mission risk assessment prior to first flight of any spacecraft as well as the need to continue to develop/refine BLEs so that they more accurately reflect the shape and material density variations inherent to the actual debris environment. The result of such activities would be spacecraft design and risk assessment processes that include more appropriate models of spacecraft response when threatened by the orbital debris environment.

Of course, the question naturally arises regarding just which BLE to use to assess the effect of an impact of a non-spherical projectile on a target structure. After all, a flake-like debris particle or a cube-like particle can impact a target at any number of different orientations, and each orientation has its own BLE. Therefore, in addition to the shape of the impacting particle, the orientation of the particle at the time of impact is of great importance to its penetrating ability. Note from Figures 22 and 23 that the impact of the cube at different orientations produces a wide variation in ballistic limit. As a result, it is important to consider the likelihood of each type of particle shape and impact orientation when performing an overall risk assessment of a spacecraft.

The likelihood of different shapes could be determined from a variety of sources, including ground-based tests, radar cross section measurements of satellite debris, and ground-based modeling of breakup events using hydrocodes or other means. The likelihood of different orientations and the effect on overall ballistic limit can be calculated using a method similar to that used in aircraft survivability analyses. In this approach, a regular solid (like a cube), can be broken into 26 views spaced at 45 degrees from one another (see Figure 25). In the case of a cube, six of the views (23%) result in a view of the cube face, 12 of the views (46%) result in a view of the cube edge, and 8 of the views (31%) result in a view of the cube corner.

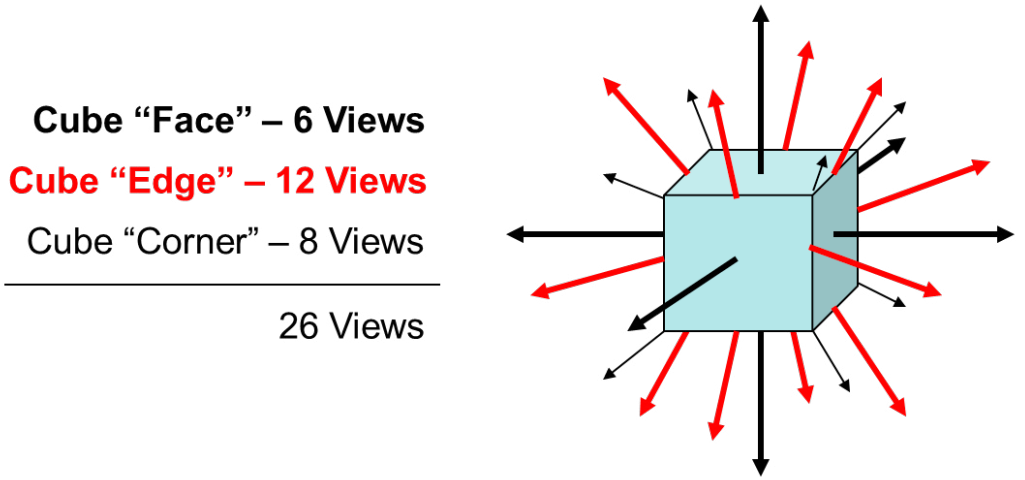

Figure 25. Impact Trajectory "Views" for a Cube

By treating these views as particle orientations coincident with the velocity vector, a weighted ballistic limit curve can be derived from individual hydrocode ballistic limit predictions for each view (or orientation). Figure 26 shows such an orientation-weighted ballistic limit curve for the cube shape

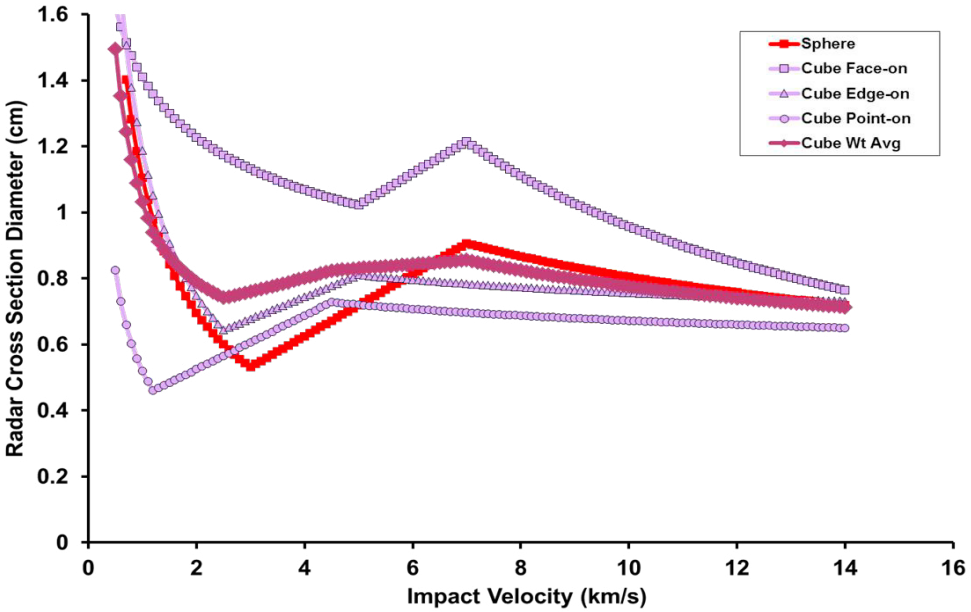

Figure 26. Original and Orientation-Weighted Ballistic Limit Curves for a Cube

6. Post-impact response characteristics

In some cases, it is equally important to know, not only whether or not a module or wall perforation will occur, but also what might be the effects of such a perforation after some time has elapsed. Of particular interest in the development of habitable spacecraft such as the international space station are the issues of late-stage structural vibrations that might result from air rushing out of a perforated module and the effects of a module perforation on its inhabitants (e.g. pressure loss, etc).

6.1 Late-stage Structural Vibrations

The perforation of a habitable module that is part of a habitable space structure in earth orbit by an orbital debris particle will result in a thrust normal to the module surface. The thrust is caused by air exhausting through the hole in the module wall created by the impact. A study was performed to examine the ensuing global dynamic response of the Space Station Freedom following such a module rupture, assuming that structural integrity would be maintained [30]. Several impact situations were considered. In each situation, the objective was to predict a worst-case response scenario. Figures 27a-c illustrate the various impact scenarios considered.

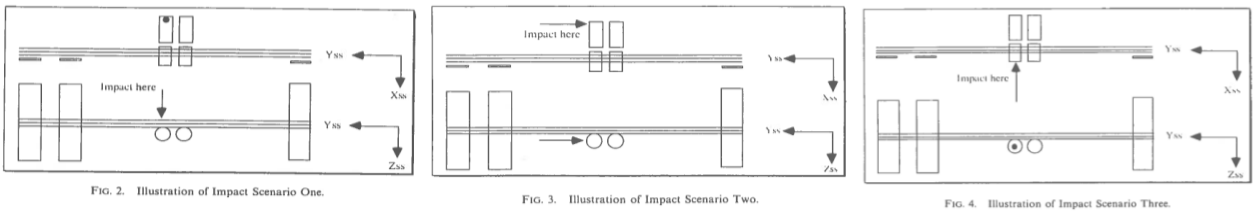

FIG. 2. Illustration of Impact Scenario One.

FIG. 3. Illustration of Impact Scenario Two.

FIG. 4. Illustration of Impact Scenario Three.

Figure 27a-c Impact Scenarios Considered in Vibration Study (from [30])

After a module wall is perforated, a thrust is generated as the pressurized air in the modules discharges into the near-zero ambient pressure space environment. This thrust is the forcing function used in the solutions of the equations of motion. Thrust histories for hole diameters of 2.5, 5, 10 and 15 cm are presented in Figures 28a,b.

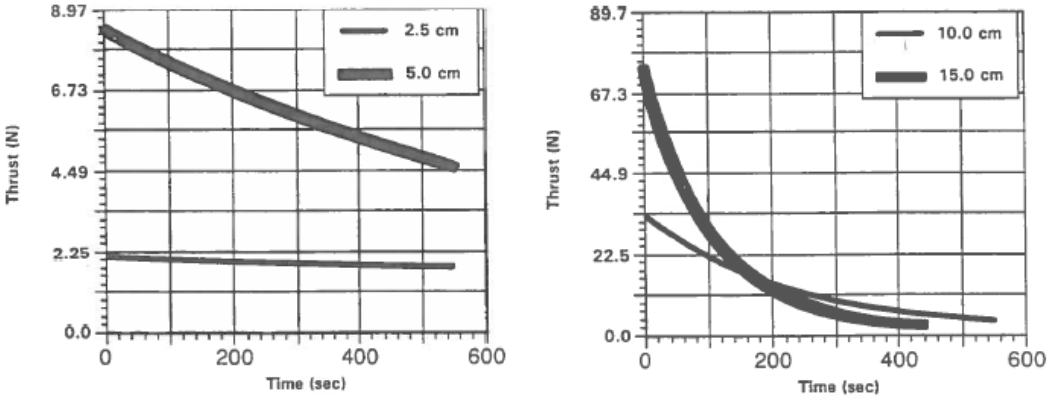

Figure 28a,b. Thrust Histories for Four Hole Diameters

The maximum vibration displacements we calculated were, admittedly, a bit smaller than we had thought would occur. However, the mass of the modules, approx. 148,860 kg, is considerable; their weight on earth is approx. 1.46 MN. The maximum calculated force value of 1472 N was quite small when compared with the weight of the clusters. Based on the results obtained, it appears that the vibration amplitudes will not compromise the structural integrity of the space station. The maximum calculated deflections following a perforating orbital debris particle impact are small (less than approx. 1.7 m) when compared to the length of the SSF from the modules to solar arrays (approx. 60 m). These findings indicate that, in the event of a module wall rupture, the survivability limitation may be a human-related factor rather than a space-station-related factor. For example, the rapid rate of de-pressurization would be serious issue, and the ability of the crew to isolate the damaged module would be critical.

6.2 Internal effects

The issue of what happens 'inside' a pressurized module following an orbital debris impact was initial considered during the Apollo program [31,32]. The issue naturally arose again during the design of the space station, only this time the habitable, pressurized volume of the station module cluster was significantly larger than that of the command module.

In an attempt to address this issue, a first-principles-based model was developed to predict the effect of a perforating orbital debris particle impact on the pressure and temperature within a pressurized habitable spacecraft module [33]. The model was developed such that it sequentially characterized the phenomena comprising the impact event, beginning with the initial impact on the outer module wall, the creation and motion of a debris cloud within the module wall system, and the impact of the debris cloud on the inner module wall. The final phase of the model was concerned with the creation and motion of the debris cloud that enters the module interior and its effect within the module on module pressure and temperature levels. This characterization is accomplished through the application of elementary shock physics theory and fundamental thermodynamic principles. Figure 29 shows a sketch of the pressure attenuation for the internal debris cloud.

The predictions of the analytical model are compared with experimental pressure and temperature data from a series of instrumented high-speed impact tests. Figure 30 shows the experimental set-up and the locations of the pressure and temperature sensors within the test chamber of the light gas gun facility that was used in the experimental program.

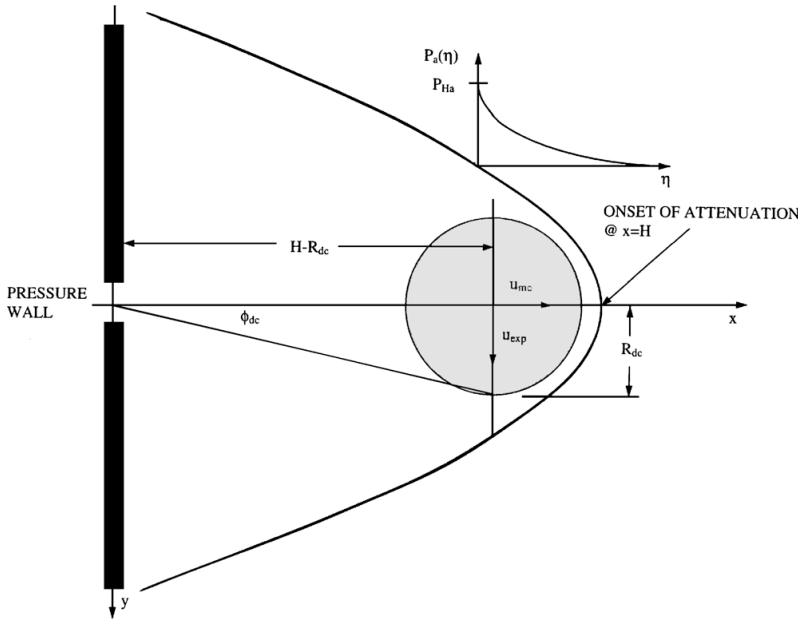

Figure 29. Pressure attenuation inside the debris cloud.

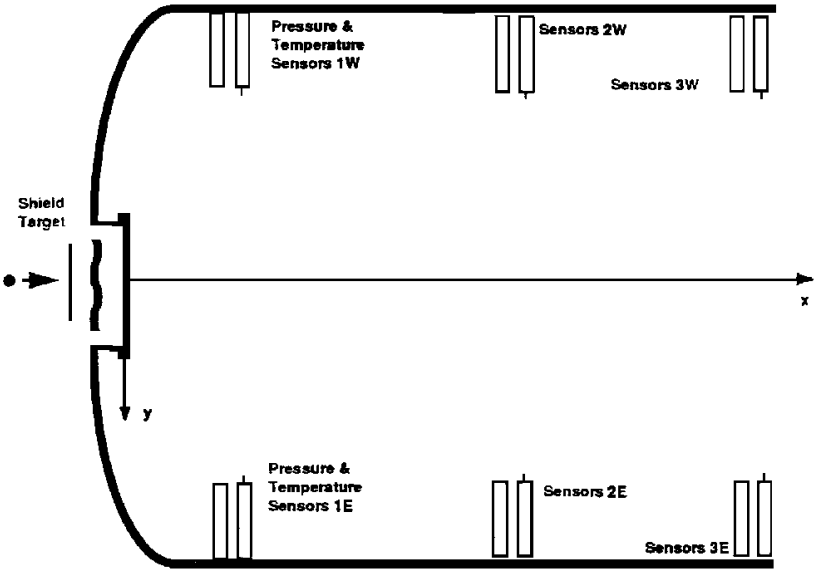

Figure 30. Pressure and Temperature Sensor Locations

Several modifications are made to the basic model to bring its predictions closer in line with the experimental results. For example, it appeared that the pressure was attenuated too rapidly by the original model, so a semi-empirical function was introduced that would ‘stretch out’ the attenuation of the pressure behind the penetrated pressure wall plate. Following the introduction of this function and the adjustment of several empirical constants, the predictions of the modified internal effects model are shown to be in close agreement with the experimental results. Table 1 shows a comparison of experimentally obtained pressure and temperature values at the locations indicated in Figure 30 and the predictions of the model developed in this study.

Table 1 Pressure and temperature prediction comparisons

	Pressure Increase		Temperature Increase	
Sensor	Experimental Result (psi)	Model Prediction (psi)	Experimental Result (deg-C)	Model Prediction (deg-C)
		Test 1		
1E	17	15.2	18	43.2
1W	18	15.2	27	43.2
2E	4	7.2	23	23.0
2W	6	7.2	20	23.0
3E	3	3.2	25	11.6
3W	2	3.2	n/a	11.6
		Test 3		
1E	21	24.3	104	63.9
1W	21	24.3	118	63.9
2E	17	17.2	139	46.6
2W	21	17.2	94	46.6
3E	8	8.0	n/a	25.1
3W	8	8.0	40	39.0
		Test 5		
1E	34	34.2	64	82.7
1W	40	34.2	54	82.7
2E	10	10.2	34	30.0
2W	15	10.2	31	30.0
3E	3	5.6	n/a	18.2
3W	4	5.6	n/a	21.5
		Test 6		
1E	16	24.6	20	64.8
1W	31	24.6	65	64.8
2E	15	17.8	52	48.1
2W	14	17.8	63	48.1
3E	12	8.3	44	25.8
3W	7	8.3	n/a	40.1

7. Impact damage characterization

In addition to being able to predict whether or not an impact will penetrate or cause critical failure of a spacecraft wall, it is also important to be able to predict the nature and extent of the penetration. Specifically, in the case of a Whipple Shield, what is the size of the hole in the pressure wall? Will it be a cookie-cutter type hole, or a bulged hole with petals accompanied by cracking? And if the latter, what is the maximum extent of the cracking? While a remote possibility, if penetration-induced cracking were to occur on-orbit, unstable crack growth could develop which could lead to an unzipping of an impacted module.

A series of studies was performed to develop empirical models of effective hole size and maximum tip-to-tip crack length for some of the multi-wall systems being developed for the international space station. The significance of the work performed is that those models could be incorporated directly into a survivability analysis to determine whether or not module unzipping would occur under a specific set of impact conditions. The prediction of hole size can also be used as part of a survivability analysis to determine the time available for module evacuation prior to the onset of incapacitation due to air loss.

Early work employed rudimentary empirical curve fits of the space station Phase B and Phase C/D test data [34]. This initial work developed equations that included a variety of the geometric parameters that define a dual-wall configuration with an internal MLI blanket. Subsequent efforts focused on specific wall constructions being considered for the international space station [35]. Pressure wall hole diameter and maximum tip-to-tip crack equations developed in this study were of the form shown in the following equation:

$$X = Af(\theta_p)g(V_p)[1- e^{-C(Mp/MBL -1)}] \quad (1)$$

where X is either hole diameter or maximum tip-to-tip crack length, respectively. In equation (1), V_p, M_p and θ_p are the velocity, mass and obliquity of the impacting projectile while M_{BL} is the ballistic limit mass at a velocity of interest for the particular system under consideration under a θ_p-degree impact. The use of projectile mass and ballistic limit

mass in equation (1) allows us to pool together the data obtained using different types of launchers. This form was chosen because (1) when using this form both hole diameter and crack length approach zero when the projectile diameter approaches the ballistic limit diameter value from above, and (2) these forms adequately represent the initial growth stage of hole diameter and maximum tip-to-tip crack length as the projectile diameter increases just beyond the ballistic limit diameters.

Figure 31 shows a comparison of the predictions of the empirical equations for maximum tip-to-tip crack length for the baseline construction of the US Lab module (i.e. Whipple Shield + MLI) and for the enhanced US Lab module wall construction (i.e. Whipple Shield + Nextel/Kevlar 'stuffing').

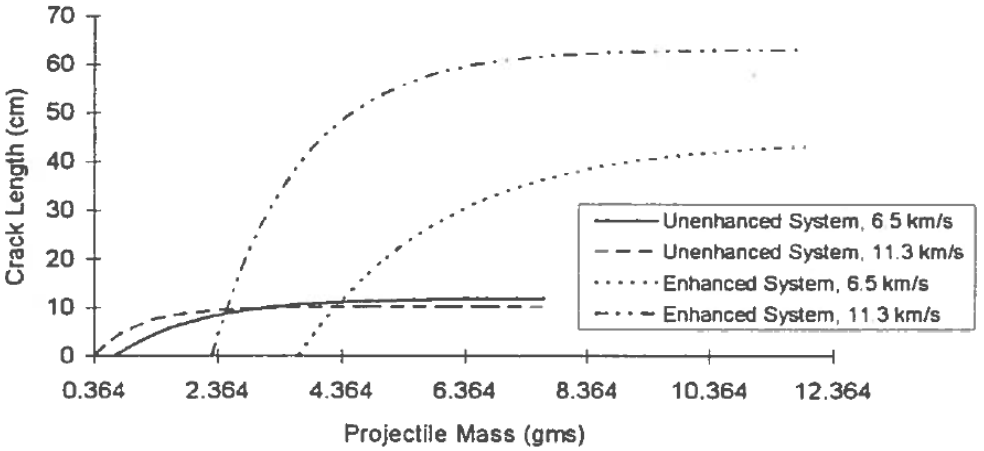

Figure 31. Comparison of Maximum Tip-to-Tip Crack Length for Enhanced and Baseline (Unenhanced) US Lab Module (Normal Impact)

The following points are evident from this figure.

1. The enhanced systems have much higher ballistic limits than baseline systems.
2. The initial slopes of the enhanced system curves are steeper than those of the baseline systems.
3. The asymptotic values of the enhanced system curves are much higher than those of the baseline systems.

These results indicate that enhanced systems, while more resistant to perforation than baseline systems, will sustain much larger cracks (and holes) – if they occur – than corresponding baseline systems, and will reach those higher values quicker. This conclusion can have serious implications when factored into risk assessments for spacecraft modules using walls of similar construction (see also [36]).

In order to be able to assess whether or not unstable crack growth could develop (leading to possible module unzipping), it is first necessary to determine whether either petalling or cracking would even occur in the event of a module perforation. A study was performed to develop an empirical model that could be used to answer this question, that is, if a pressure wall were perforated, would the perforation be in the form of a petalled hole or a cookie-cutter hole? The resulting model was a petalling limit function (PLF) that predicts the onset of petalling in terms of impact conditions and spacecraft wall system geometry [37]. In a sense, it is analogous to the ballistic limit equation (BLE) that predicts the onset of pressure wall failure or perforation in terms of the same parameters.

Figures 32a,b and 33a,b show plots of the ballistic limit equation (BLE) and petalling limit function (PLF) for these two baseline lab cylinder (BLC) and enhanced lab cylinder (ELC) wall systems for 0-deg and 45-deg impact trajectories, respectively. Also shown in these figures are the results of experimental tests with regard to whether a pressure wall perforation was in the form of a petalled hole or a cookie-cutter hole.

As can be seen from Figures 32a,b, for the BLC wall system, there exist projectile diameter-impact velocity combinations that are above the ballistic limit curve but below the petalling limit curve (shown as region A in Figures 32a,b). In this region, perforation of the pressure wall in a BLC wall system would result in cookie-cutter holes. However, above the petalling limit function (region B in Figures 32a,b), the intensity of the impact loading is such that pressure wall perforation would most likely be accompanied by petalling and cracking. We note that the scatter in the data in Figure 32a is not new or surprising. In fact, it is consistent with the scatter in the data used to obtain ballistic limit curves for similar multi-wall systems under similar impact conditions.

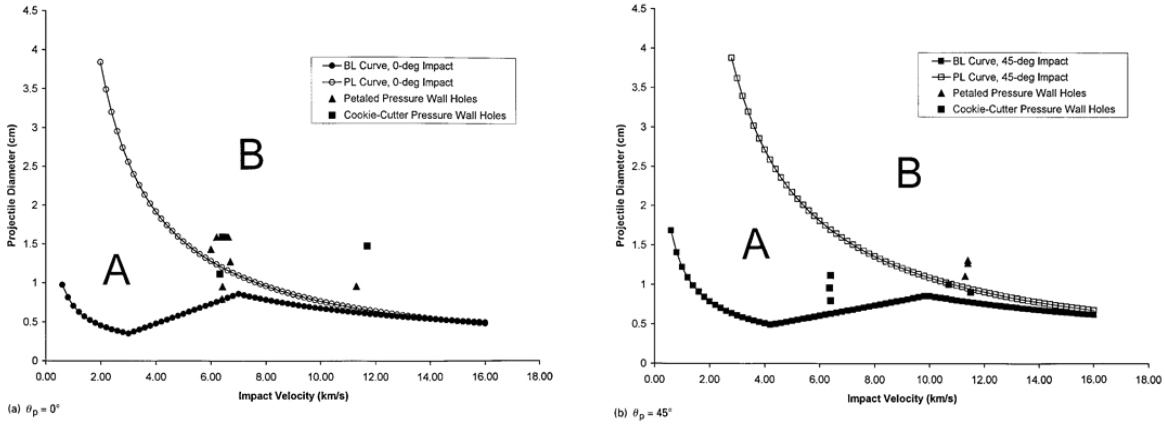

Figure 32a,b. Ballistic Limit Equation (BLE) and Petalling Limit Function (PLF) Curves for the Baseline US Lab Cylinder (BLC) Wall System

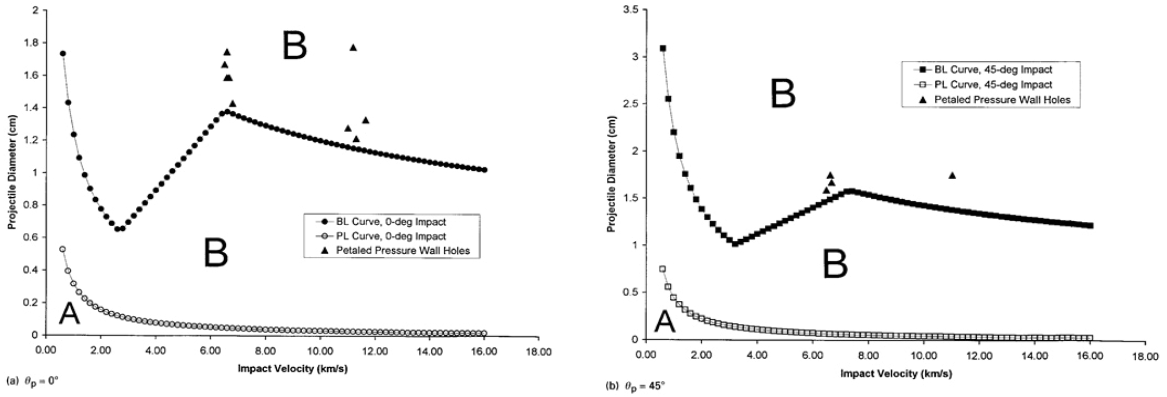

Figure 33a,b. Ballistic Limit Equation (BLE) and Petalling Limit Function (PLF) Curves for the Enhanced US Lab Cylinder (ELC) Wall System

With regard to the ELC wall system, Figures 33a,b show that the petalling limit function is always below the ballistic limit curve. Hence, pressure wall perforations in an ELC wall system will always be accompanied by petalling and cracking, even at relatively low impact velocities. This is borne out by the experimental data in Figures 33a,b, which show only petalled perforations. Thus, the model developed shows that the perforation of a spacecraft wall with an enhanced shield will always be accompanied by petalling and cracking, while the perforations of a Whipple-type spacecraft wall may or may not be petalled and cracked, depending on impact conditions.

Parallel to these empirical modelling efforts, we also sought to develop an analytical, first principles-based model of hole diameter and maximum tip-to-tip crack length for a spacecraft module pressure wall that has been perforated in an orbital debris particle impact [38]. The analytical hole diameter and crack length models were developed by sequentially characterizing the phenomena comprising a normal impact event. These phenomena include the initial impact, the creation and motion of a debris cloud within a multiwall system, the impact of the debris cloud on the pressure wall, pressure wall deformation prior to crack formation, pressure wall crack initiation, propagation and arrest, and finally, pressure wall deformation following crack initiation and growth. Two types of multi-wall systems were considered: a Whipple-type system (where the inner wall is a multi-layer thermal insulation blanket) and an enhanced shielding system (where the inner wall consists of several layers of Kevlar and Nextel cloth added to an MLI blanket).

As noted previously, some perforated pressure walls holes retained their flatness and contained what may be

called "cookie cutter holes", that is, holes with jagged edges from which pressure wall material had been simply punched out. Others were bulged with petals and extensive cracking. The model developed, therefore, also included the PL function described above as a means of determining, a priori, whether a pressure wall perforation would be in the form of a petalled hole or a cookie-cutter hole. Figure 34a,b shows a graphical representation of the early (just perforated) and late (petalled) stages of the deformation of a pressure wall plate that is impacted and perforated impulsively.

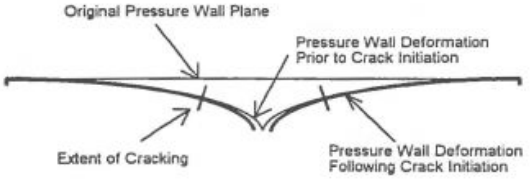

Fig. 4. Pressure wall deformation following crack initiation.

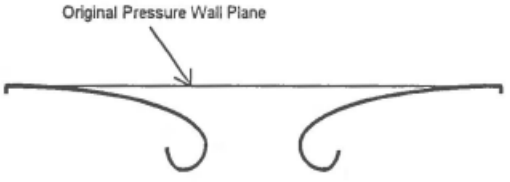

Figure 5. Advanced Stage of Pressure Wall Cracking with Petals Shown

Figure 34a,b. Graphical Representation of the Pressure Wall Deformation and Petalling Model

The table in Figure 35 shows how well the model was able to predict the hole diameter and crack length in several impact tests for three wall configurations. Model predictions compared fairly well with experimental results, but especially well for those tests highlighted in a red outline in Figure 33. This hole and crack length prediction model was then extended to oblique impacts with similar results (see the table in Figure 36 below [39]).

Table 3. Comparison of modified model predictions and actual empirical data

Wall System	*Test No.*	*V_p (km/s)*	*d_p (cm)*	*Hole Diameter (cm)*			*Crack Length (cm)*		
				Exp. Res.	*Model Pred.*	*Emp. Eqn.*	*Exp. Res.*	*Model Pred.*	*Emp. Eqn.*
	HS-11	6.41	0.95	3.25	7.69	2.70	5.66	3.50	3.34
BLC	7698-1	11.70	1.47	3.96	1.81	4.05	10.29	10.97	10.94
	1722	6.78	1.42	11.20	3.98	3.43	32.39	8.79	10.04
ELC	7698-3	11.64	1.32	22.17	22.91	20.79	41.91	39.35	45.11
	1699	6.67	1.42	7.12	6.46	5.93	18.67	19.59	18.76
LEC	7698-7	11.37	1.32	6.25	4.04	7.68	13.72	14.15	23.49

Figure 35. Comparison of Model predictions and Experimental Results, Normal Impact

Table V. Comparison of modified model predictions and actual empirical data.

Wall system	Test no.	θ_p (deg)	V_p (km/s)	D_p (cm)	D_{eq} (cm)			L_{tt} (cm)		
					Exp. res.	Model pred.	Emp. eqn.	Exp. res.	Model pred.	Emp. eqn.
BLC	HS-15	45	6.40	1.11	2.74	3.08	3.05	3.63	6.35	6.67
ELC	n/a	45	← All diameters tested exceeded maximum allowable limit of 1.27 cm. →							
LEC	1691	45	6.62	1.18	1.22	4.57	4.77	9.91	8.08	8.42

Figure 36. Comparison of Model predictions and Experimental Results, Normal Impact

Most recently [40], we updated the 1997 hole diameter and crack length equations (dubbed the S-W Model) by making them more general and by extending them to diameters and masses significantly beyond the ballistic limit of

the system being impacted (called the W-S model). A generic hole diameter-vs-projectile diameter curve is shown in Figure 37 for a given impact velocity, trajectory obliquity, and shield system geometry. The general type of phenomenology shown in Figure 37 is broken up into 3 regions; each region corresponds to a certain type of projectile response and pressure wall hole growth pattern. The shape of the curve shown in each of these three regions is based on the following considerations.

(1) Initially, the hole diameter (and the cracking) phenomena are governed by the nature of the debris cloud loading on the module pressure wall. This case corresponds to Region I of the curve shown in Figure 37. In Region I, the projectile is completely shattered upon impact and the degree of fragmentation increases with increasing projectile diameter. As a result, spread of the debris cloud created by the initial impact also increases as does the effective diameter of the hole in the pressure wall.
(2) At a certain projectile diameter (labeled D1 in Figure 37), the projectile is too large for it to be completely shattered by the outer bumper or shielding system. Hence, for projectile diameters beyond this point (i.e. in Region II), the amount of projectile fragmentation decreases with increasing projectile diameter as does the spread of the debris cloud and the size of the hole in the pressure wall.
(3) In Region III (i.e. for Dp >> D2), the projectile diameter is very large when compared to the ballistic limit diameter value, perhaps even as large as the spacing between the bumper and the pressure wall. In such cases, the multi-wall system can be expected to act as a single thin plate. Hence, the form of that part of the curve should be similar to that generated by single plate hole diameter equations. In this case, the pressure wall hole diameter again increases with increasing projectile diameter.

Figures 37 and 38 present a sketch of the three-part equation (thick solid line) that we used as the basis for the W-S model developed to model the response regimes as outlined above, and the implementation of the full model for the US Lab Cylinder dual-wall system.

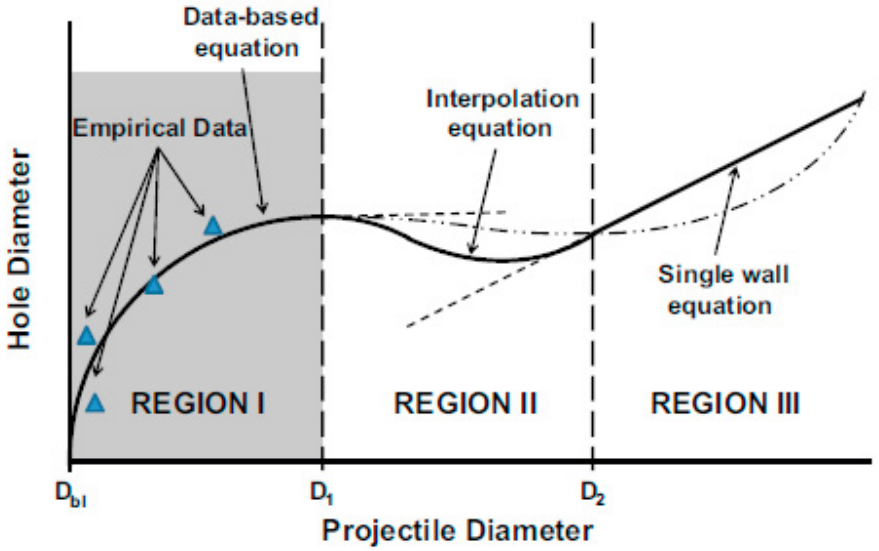

Figure 37. Sketch of a Three-part Hole Diameter or Crack Length Equation

We found that the predictions of the new W-S model fit the empirical data just as well as, if not better than, the previous S-W model and that the W-S model displayed the appropriate phenomenological hole size and crack length response characteristics as the diameter of the impacting projectile increased beyond the ballistic limit of a particular wall system. Based on these results, we believe that the new W-S hole and crack size model encoded will improve the fidelity of risk assessments performed for the international space station or other spacecraft with similar wall configurations.

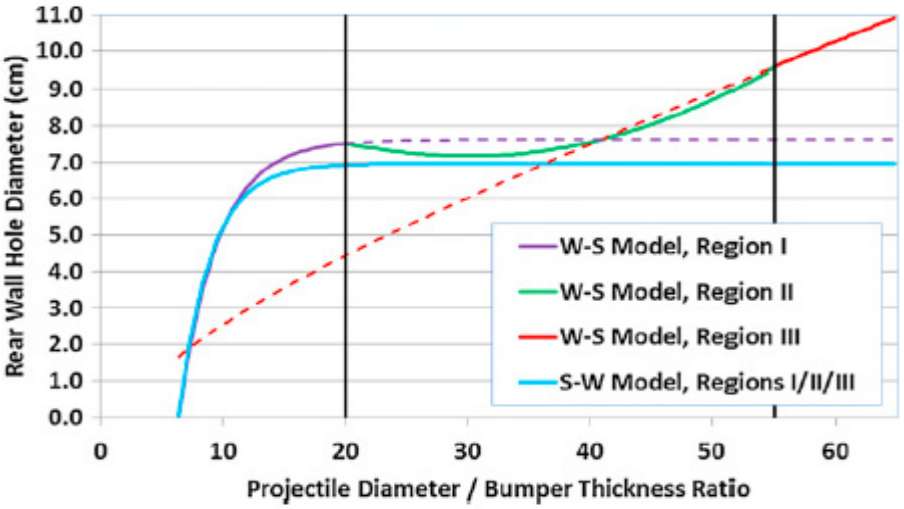

Figure 38. Plot of the W-S Rear Wall Hole Diameter Prediction Model,
US Lab Cylinder Wall System, 6.5 km/s Impact, 0-deg Trajectory Obliquity

8. Uncertainly analysis

All of the studies we have performed have been heavily reliant on data, whether as the basis for empirical or semi-empirical response prediction models or against which the predictions of analytical models are compared. However, as we saw in Figures 12a,b and 26 a,b there can be quite a bit of scatter amongst high speed impact test data – it doesn't always fall neatly into place. This gives rise to questions regarding our certainty of whatever information we extract from high speed impact tests and how repeatable it is, or put another way, what is the uncertainty in the results obtained in hypervelocity impact tests? Reporting uncertainty information enables those performing MMOD risk assessments to fold uncertainty information into those assessments, thereby putting them in perspective with the other risk contributors. Risk predictions can also be used to help prioritize research programs to reduce the highest contributors to risk and uncertainty first.

Initial efforts focused on assessing the repeatability of light gas gun information [41]. A review of the Phase B and Phase C/D impact test parameters revealed that very few of the impact tests were repeated under the same impact conditions. Thus, a traditional repeatability analysis of the phenomena involved in the response of dual-wall structures to hypervelocity projectile impact was impossible to perform. A modified repeatability analysis was then performed by pooling together several related groups of similar tests. This resulted in sample sizes of at 5-10 related tests per group. Though the pooled test groups were by no means large, some sort of comparison and assessment of phenomena repeatability became possible.

For example, one such grouping was all tests performed on dual-wall structures without MLI and with a 1.6-mm-thick bumper, a 3.175-mm-thick pressure wall, and a 10.16-cm stand-off distance. Within that group, tests were then paired according to similarity in projectile diameter, trajectory obliquity, and impact velocity. Using the test pairs and groupings so created, a quantifiable level of repeatability for dual-wall systems tested in the NASA/MSFC light gas gun was determined by calculating the number of test pairs within a group of tests that did or did not sustain pressure wall perforation or rear-side spall in both tests of each test pair. The repeatability for that group of tests was then stated as the percentage of test pairs that were in agreement with regard to pressure wall perforation or rear-side spallation. This quantity was referred to as the repeatability index (RI) for the specific group of tests under consideration. In the end, we found that that the perforation RI was approx. 75%. In other words, in approx. 75% of the test pairs considered, either both walls were perforated, or both walls were not.

NASA currently uses the BUMPER code to calculate the risk of MMOD penetration for the International Space Station (ISS), extravehicular activity (EVA) suits, and other spacecraft. While BUMPER is a powerful tool, one of its limitations is that it provides a point estimate of MMOD risk with no assessment of its associated uncertainty. One reason for this is that the uncertainties associated with input models underlying BUMPER are largely unknown.

These underlying models include damage prediction / ballistic limit equations, environment models, and failure criteria definitions. In order to attempt to quantify the overall uncertainty bounds on MMOD risk predictions, the uncertainty in these three areas must be identified. In a more recent study [42,43], we presented several possible approaches through which uncertainty bounds and/or confidence intervals could be developed for the various damage prediction (DP) and ballistic limit (BL) equations encoded within BUMPER.

The DP equations in BUMPER are curve-fits to empirical data, that is, they are the results of statistical regression analyses of available test data. As such, uncertainty bounds and/or confidence intervals can readily be obtained at the time that the regression analyses are being performed to form the DP equations. However, unlike DP equations, BL equations are not statistically based. They are *not* curve-fits, but are rather simply lines of demarcation between regions of penetration and non-penetration in regions where test data exist. In regions where test data does not exist, lines are drawn based on assumed forms and assumed exponents of various terms. As a result, and also *un*like the DP equations, it is simply *not* possible to obtain uncertainty bounds and/or confidence intervals as part of the current procedure that is used to derive the BL equations. Alternative, innovative approaches must be developed to either (i) obtain the required uncertainty information from existing BL equations and the data on which they are based, or (ii) re-derive the BL equations using a statistics-based approach so that uncertainty information is forthcoming out of the analyses along with the equations themselves.

9. Debris cloud characterization

The key to conducting an accurate damage assessment of a target impacted by a high speed projectile is the use of a robust assessment methodology. To accurately determine total target damage, a damage assessment methodology must include the effects of discrete impacts by solid debris cloud fragments as well as impulsive loadings due to molten and vaporous debris cloud material. As a result, the amount of debris cloud material in each of the three states of matter must be known to accurately assess total target damage and break-up due to a high speed impact. To begin addressing this need, a first-principles based model was developed [44] to calculate:

- the amount of material in a debris cloud created by a perforating hypervelocity impact that is solid, molten, and vaporous;
- the debris cloud leading edge, trailing edge, center-of-mass, and expansion velocities; and,
- the angular spread of the debris cloud material.

Figure 39 shows a sketch of a debris cloud as well as characteristic velocity parameters of interest. These quantities were calculated using conservation of mass, momentum, and energy together with equations of state for the bumper and projectile materials.

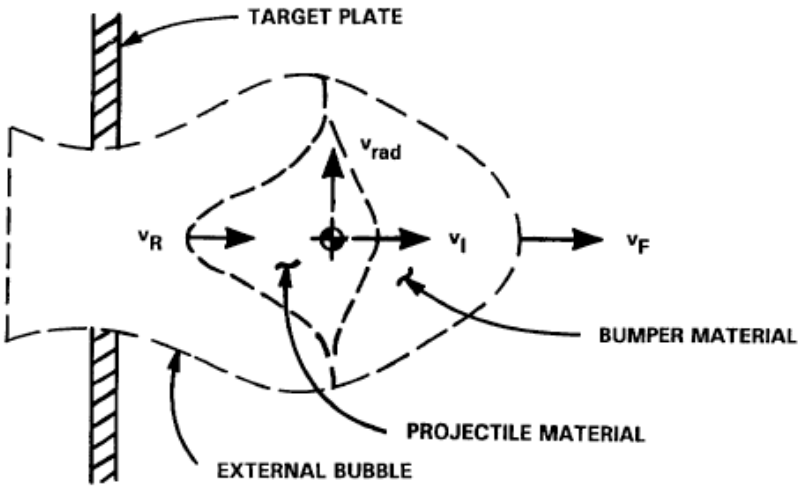

Figure 39. Sketch of Debris Cloud with Expansion Velocities

The shock pressures, energies, etc., in the projectile and target materials are calculated using the three one-dimensional shock-jump conditions, a linear relationship between the shock wave velocity and particle velocity in each material, and continuity of pressure and velocity at the projectile-target interface. Solving the resulting equations simultaneously yields expressions for projectile and target particle velocities that are then used to calculate shock velocities, pressures, internal energies, and material densities after the passage of a shock wave.

Although the shock loading of a material is an irreversible process that results in an increase of the internal energy of the shocked material, the release of a shocked material occurs isentropically along an "isentrope" or "release adiabat." The difference between the area under the isentrope and the energy of the shocked state is the amount of residual energy that remains in the material and can cause the material to melt or even vaporize. To calculate the release of the projectile and target materials from their respective shocked states, an appropriate equation-of-state is needed for each material. To keep the analysis relatively simple, the Tillotson equation-of-state was used.

Once the residual internal energies in the shocked and released portions of the projectile and target materials are obtained, the percentages of the various states of matter in the resulting debris cloud are estimated using fundamental thermodynamic relationships between energy, specific heat, and temperature.

The table in Figure 40 compares the predictions of this model against numerical and empirical results obtained in previous studies of debris cloud formation. It is evident that the model did quite well in matching previous results for the projectile types, target characteristics and impact velocities considered.

Table 1. Comparison of DEBRIS3 with Empirical Results and 1-D Hydrocode Predictions

T	m_p	v_o	v_f/v_o			v_i/v_o			v_r/v_o			v_{exp}/v_o	
(mm)	(g)	(km/s)	(1)	(2)	(3)	(1)	(2)	(3)	(1)	(2)	(3)	(1)	(3)
Effect of Target Thickness													
1.0	1.0	6.39	1.44	1.41	1.40	0.91	0.89	0.89	0.36	0.34	0.34	0.24	0.27
1.5	1.0	6.36	1.44	1.41	1.40	0.88	0.83	0.84	0.36	0.34	0.34	0.24	0.32
2.0	1.0	6.38	1.42	1.41	1.40	0.83	0.79	0.79	0.35	0.34	0.33	0.27	0.36
2.5	1.0	6.53	1.46	1.41	1.40	0.79	0.76	0.75	0.35	0.34	0.33	0.27	0.38
Effect of Impact Velocity													
1.5	1.0	3.45	1.37	1.39	1.39	0.86	0.84	0.84	0.43	0.36	0.36	0.23	0.33
1.5	1.0	4.85	1.43	1.40	1.39	0.87	0.84	0.84	0.39	0.35	0.35	0.23	0.33
1.5	1.0	6.36	1.44	1.41	1.40	0.88	0.83	0.84	0.36	0.34	0.34	0.24	0.32
Effect of Projectile Mass													
2.0	1.0	6.38	1.41	1.41	1.40	0.83	0.79	0.79	0.35	0.34	0.34	0.27	0.36
2.9	3.0	5.66	1.44	1.40	1.40	0.82	0.80	0.79	—	0.34	0.34	0.23	0.36
4.4	10.0	5.12	1.40	1.40	1.39	0.83	0.80	0.79	0.36	0.35	0.35	0.22	0.37

(1) Experimental Results (Piekutowski, 1990).
(2) 1-D Hydrocode Predictions (Piekutowski, 1990).
(3) DEBRIS3 Predictions.

Figure 40. Comparison of Model Predictions with Numerical and Experimental Results

Following on the success of using 1-D shock physics and elementary mechanical and thermodynamic principles in modelling normal impact, we decided to investigate whether or not it would be possible to apply this approach to oblique impact. Figure 41 shows a sketch of an oblique impact on a thin plate along with the parameters that characterize the debris clouds that are created as a result of such an impact.

As can be seen from Figure 41, the number of unknowns to be determined to completely characterize the three debris clouds is twelve: three debris cloud masses, three axial velocities, three expansion velocities, and three center-of-mass trajectories. Conservation of mass, energy, and momentum (horizontal and vertical) provide four equations, far short of the twelve required. A shock physics-based model of the impact was developed to provide additional information that can be used to determine these twelve quantities.

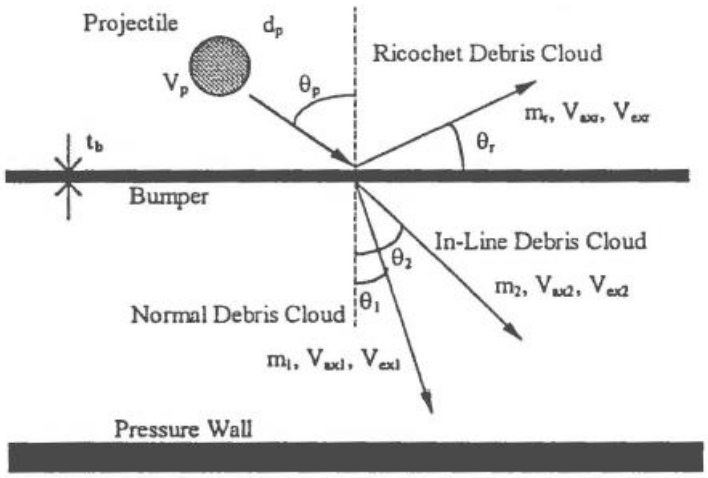

Figure 41. Oblique High Speed Impact of a Dual-Wall Structure

Early efforts focused on attempting closed-form (or nearly closed form) solutions involving the conservation equations and elementary shock physics equations (see, e.g. [45] and [46]). These initial efforts were not as successful as hoped for, and required the introduction of a large number of empirical constants. In an attempt to reduce the reliance of such approaches on empirical parameters, we endeavored to use oblique shock wave theory as a means of directly obtaining some of the debris could velocity and trajectory parameters shown in Figure 41 [47]. Figures 42a,b illustrate the parameterization of the various penetrating and ricochet shock waves created in the impact. Figures 43a,b,c show comparisons between the predictions of the model for the three trajectory angle and numerical and experimental results. While the trends predicted by the model compared favorably with the experimental results, there were some discrepancies in the actual values of the various center-of-mass trajectories. A possible reason for the discrepancies is the assumption of pure hydrodynamic behavior in the model development.

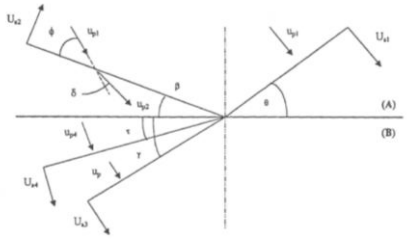

Fig. 4. Oblique incidence of a shock wave at an interface between two dissimilar materials, double transmitted wave mechanism, unsteady coordinate system.

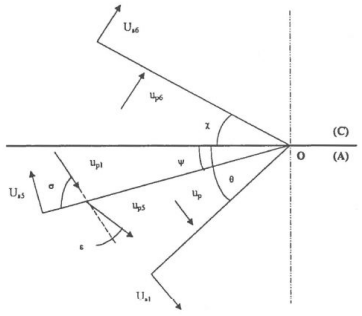

Fig. 5. Wave configurations for ricochet mechanism, unsteady coordinate system.

Figure 42a,b. Oblique Shock Wave Characterizations

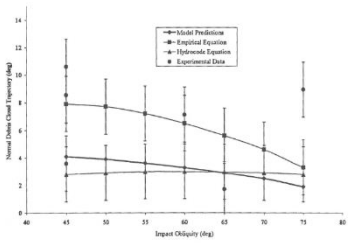

Fig. 6. Comparison of model predictions with experimental and hydrocode results for θ_1.

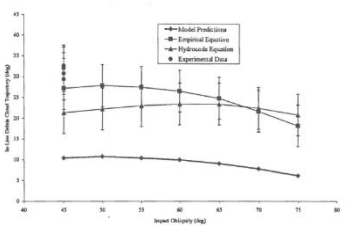

Fig. 7. Comparison of model predictions with experimental and hydrocode results for θ_2.

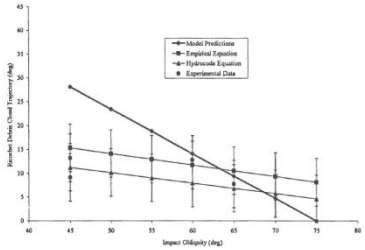

Fig. 8. Comparison of model predictions with experimental and hydrocode results for θ_r.

Figure 43a,b,c. Model Predictions, Numerical Results, and Empirical Data Comparisons

10. Pressurize vessels

Most spacecraft have at least one pressurized vessel on board. For robotic spacecraft, it is usually a liquid propellant tank, while for human spacecraft there are the pressurized living quarters (or modules). Although considerable energy and effort has been expended in the study of the response of non-pressurized spacecraft components to these kinds of impacts, relatively few studies have been conducted on the pressurized elements of such spacecraft. Several studies were performed [48] in an effort to address several aspects of this problem, including:

- an examination of how well current BLEs predict damage that might occur in pressurized spacecraft components,
- the development of general, data-driven equations that differentiate between impact conditions that would result in only a small hole or crack in a pressurized tank from those that would cause catastrophic tank failure, and
- the development of a first-principles based model that predicts whether or not cracking might start or a through-crack might result under a crater in a thin plate.

10.2 Effect of internal stress fields on ballistic limit

When we first looked at whether or not the BLEs derived using unstressed plates were applicable to stressed plates, we found that (1) for the most part, if an unstressed plate was penetrated, so was the corresponding stressed plate (and vice versa), and (2) the size of the perforation as well as the extent of cracking did show some dependence on the presence of the inner wall stress field [49]. However, no comparisons were made against BLE predictions since at the time of that study NASA had not yet put forth a vetted and calibrated BLE for dual-wall systems. Such BLEs now exist for many different types of dual- and multi-wall configurations.

In this study, the data in [49] was re-analyzed and compared against the predictions of the 1993 and 2001 NASA BLEs for aluminum dual-wall systems (i.e. those in Refs. [50] and [51], respectively). Figure 44 shows a comparison of 0-deg impact P / NP data against the NASA BLEs, while Figure 45 shows the comparison for 45-deg impact obliquities.

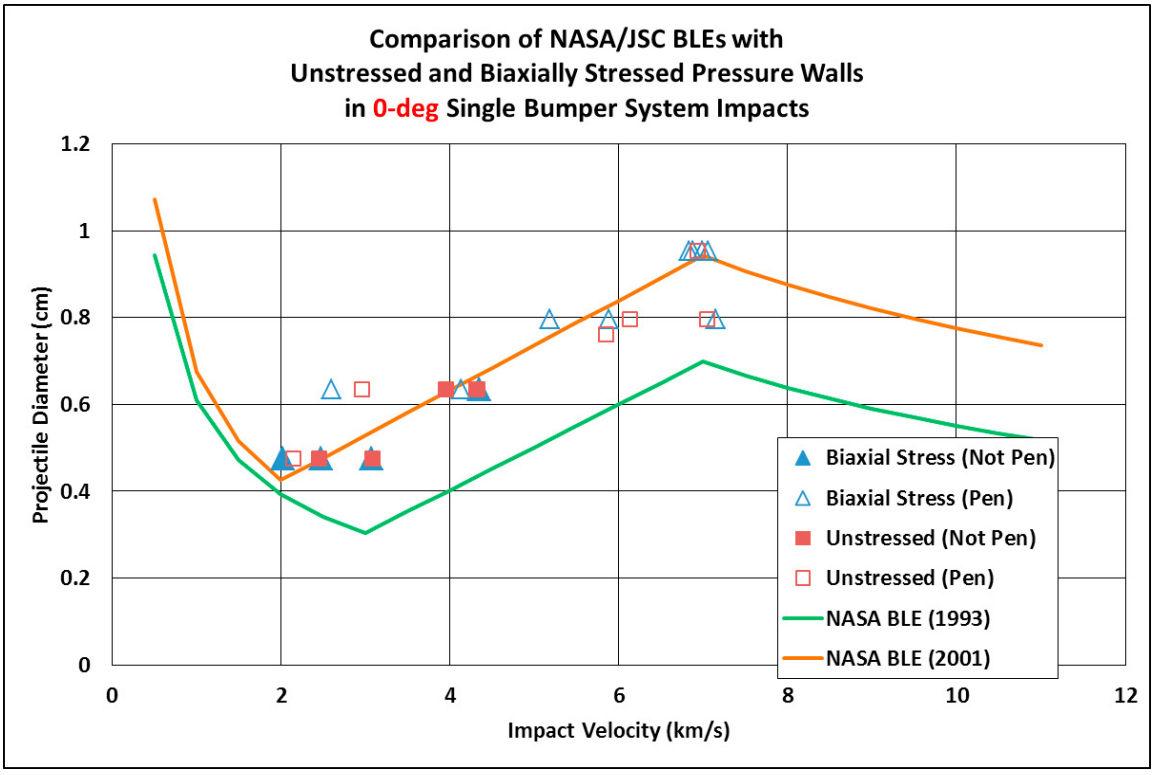

Figure 44. Comparisons of Test Data vs BLE Predictions, 0-deg Impacts

From these figures we see that:

- For relatively low internal pressures, the presence of an internal stress field does not appear to have any significant effect on whether or not the inner wall of a dual-wall configuration will be penetrated following a hypervelocity impact.
- It is not possible to say at this time whether or not the same holds true for spacecraft components under much higher internal pressures. The reason for this is that the primary objective of nearly all of the testing performed with high pressure vessels or tanks was to study what would happen *WHEN* the tanks were perforated, and not to determine *IF* they would be perforated.
- The 2001 BLE appears to perform reasonably well in predicting the P / NP response of dual-wall systems with stressed inner walls for the particular stress state considered. However, it appears to be less conservative than might be acceptable since it predicts as non-penetrating several impacts that did actual penetrate the rear wall.

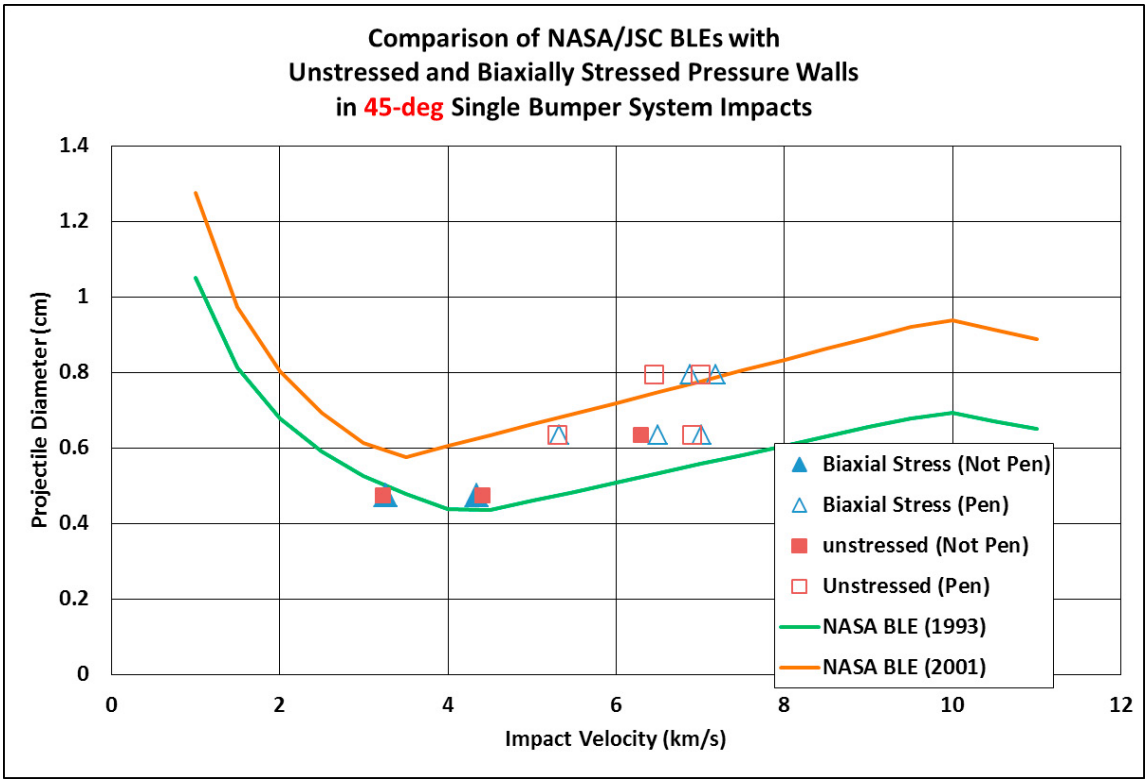

Figure 45. Comparisons of Test Data vs BLE Predictions, 45-deg Impacts

10.3 Tank perforation vs rupture

Of specific interest in this study was whether a high-speed impact would cause a tank to rupture (i.e. a catastrophic failure), or if it merely would result in an entry hole or entry and exit holes. This is an important consideration in the design of a pressurized tank – if possible, design parameters and operating conditions should be chosen such that additional sizable debris (such as that which would be created in the event of tank rupture or catastrophic failure) are not created as a result of an on-orbit MMOD particle impact.

The objective of the work that was performed was to develop empirically-based equations that could be used to determine whether or not a particular set of impact parameters under a specified operation condition would result in the rupture of the tank [48]. To render the equations as broadly applicable as possible, the operating conditions (x-axis) were parameterized as the hoop stress in the tank (normalized with respect to the ultimate stress of the tank wall

material), and the impact conditions (y-axis) were parameterized as impact energy (normalized with respect to a number of appropriate tank wall material properties). Figure 40 is a plot of this data for radially impacted, unshielded, cylindrical metallic tanks, showing which tests resulted in tank rupture (red data points) and which did not (green data points).

Also plotted in Figure 46 are some possible forms of demarcation lines between tests that did not result in tank rupture (green data markers) and tests that did (red data markers). In Figure 40 it is evident that a linear demarcation line would not be feasible and that an exponential line would have only limited applicability; however, a power law curve does appear to work quite nicely.

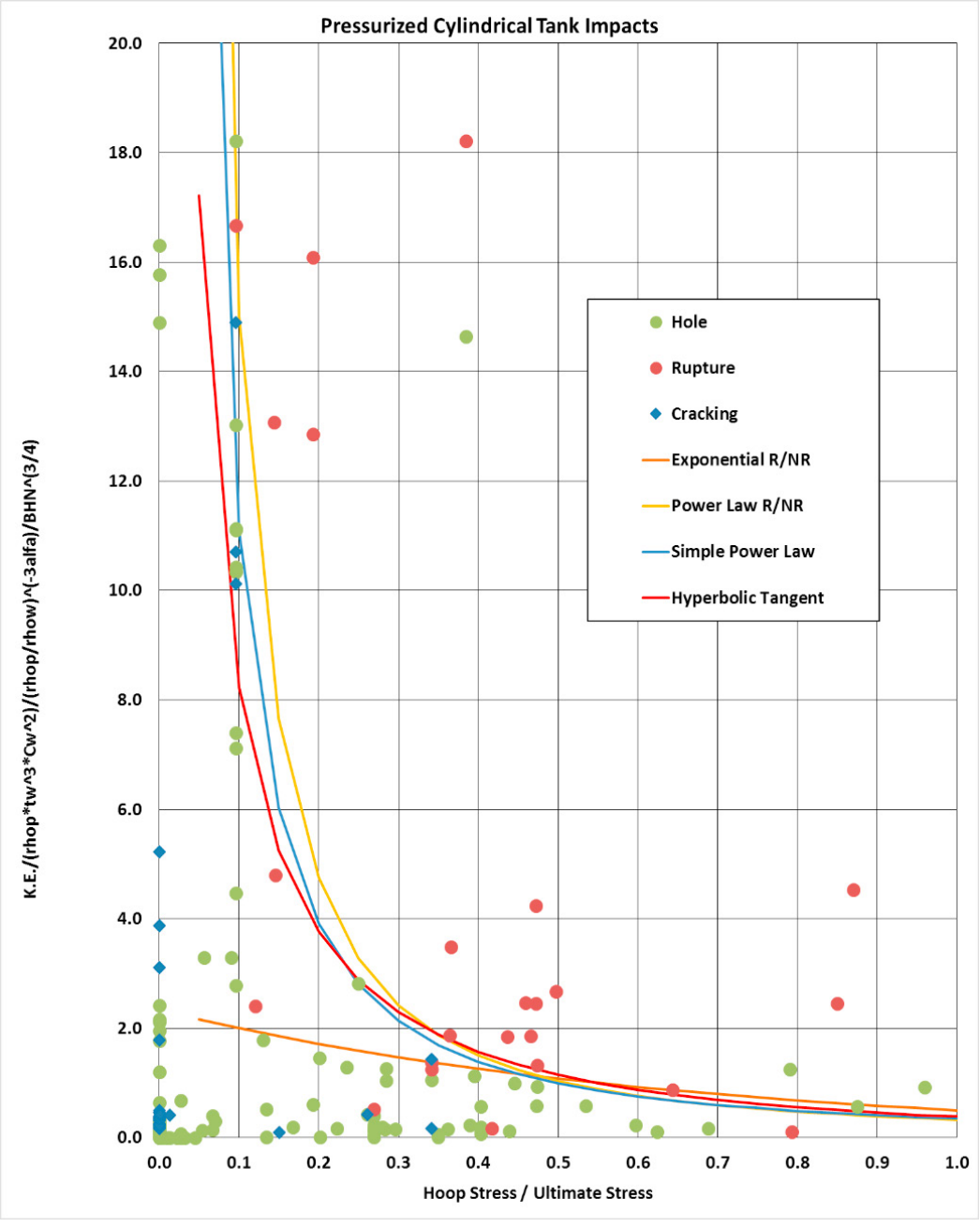

Figure 46. Rupture / Non-Rupture Response of Radially Impacted Cylindrical Metallic Tanks

10.4 Analytical modelling

Pressurized tank wall failure following a high-speed impact can occur in any number of ways. In the event of a tank wall perforation, these failure mechanisms include

a. a through-hole on the front-facing tank wall (with only pitting on the inside of the rear surface),
b. a through-hole on the front and on the rear walls, or
c. so-called 'wing cracks' that emanate from a through-hole on either the front or rear wall (these cracks could lead to catastrophic failure of the tank, but not necessarily).

Even if tank perforation does not occur (that is, the front wall sustains only crater damage), it is possible that a crack might emanate from the floor of one of the deeper craters, and, under the right conditions, grows through the tank wall until it reaches the rear surface of the front wall. While the failure modes associated with tank perforation (and longitudinal cracks that might develop from the edges of such perforations) have been studied extensively by other investigators, tank failure resulting from a crack forming at the floor of a deep crater or pit has not.

The latter tank failure mode (i.e. failure due to cracking without perforation) appears to be linked to the design criteria currently used by NASA and its contractors to design pressurized tanks. As such, the objective of this study was to develop a first-principles based model that can be used to assess the effect of penetration depth on the possibility of a crack forming under a crater, and whether or not the crack might grow through the tank wall thickness [52]. Figure 47 highlights the various components of this model and shows the flow of the calculations performed.

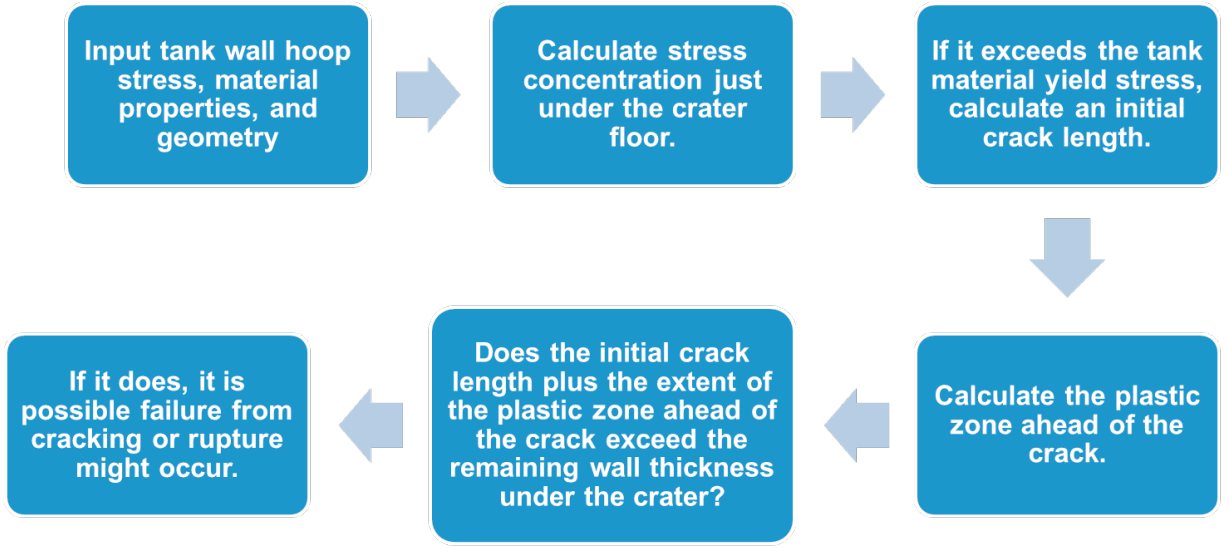

Figure 47. Flow of Calculations in Cracking Formation Model

Figure 48 shows the plot obtained by running the model for Ti-6Al-4V tanks for a series of penetration depths relative to tank wall thickness and a series of operating conditions (hoop stress relative to material yield stress). Figure 46 highlights the nominal operating condition of the SMAP satellite currently being built as well as where the results of some experimental tests from [53] and [54] might lie when the model is run using the conditions of those tests. In Figure 46, we see that the phenomenology evident in experimental data agrees with the predictions of the model developed herein:

a. the tests (purple square markers) that resulted in tank wall cratering without rupture (but possibly cracking under the crater) [53] fall in the regime where the model predicts that cracking might occur under a crater, but not loss of pressurization, and
b. the test (teal triangle) that resulted in tank rupture [54] falls in the regime where the model predicts that the length of the initial crack plus the plastic zone ahead of it will likely exceed the thickness of the tank wall material under the crater.

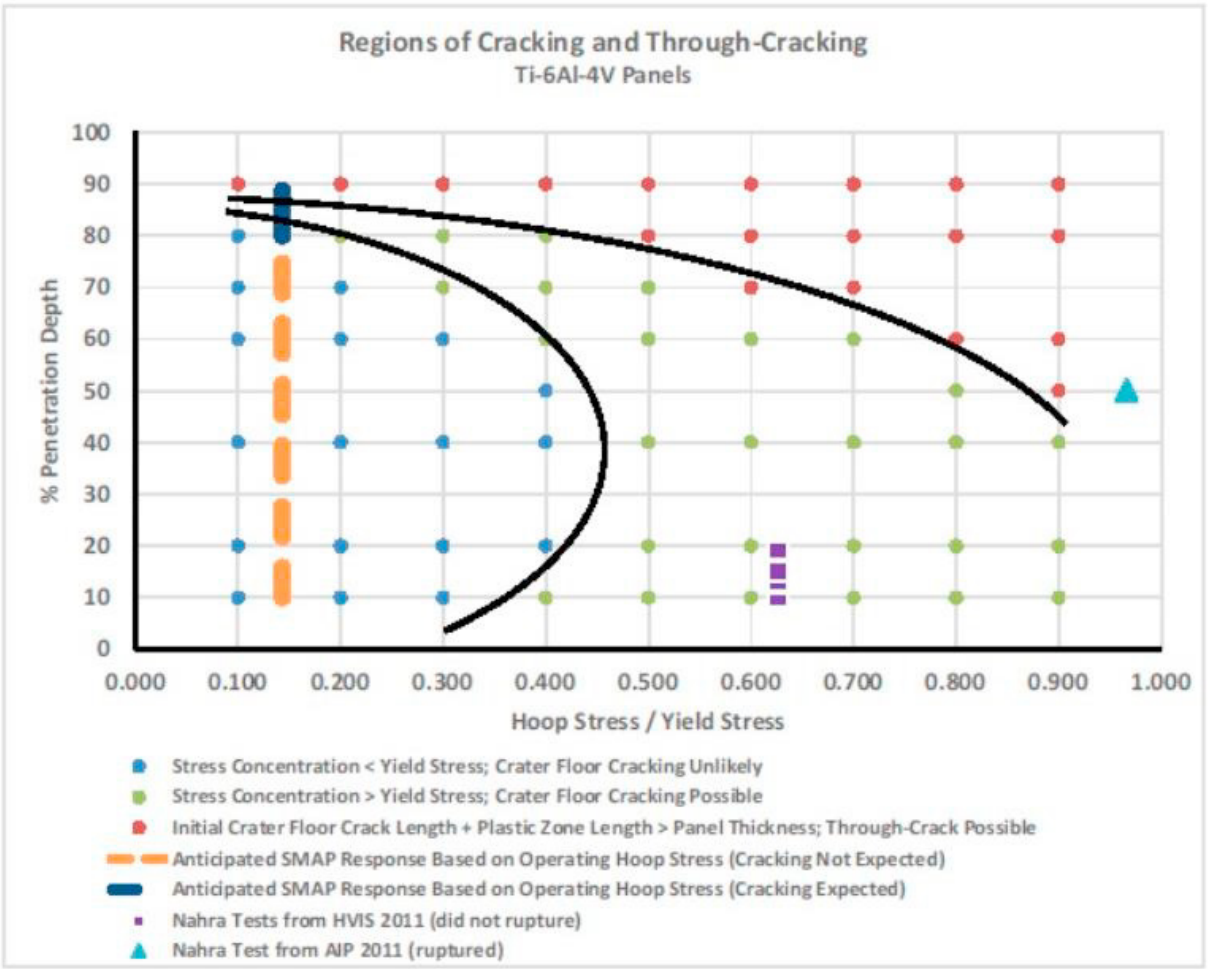

Figure 48. Model Predictions of Regions of Cracking and Through-Cracking for Ti-6Al-4V Tank Walls

11. Other Studies and Recent Efforts

In addition to the studies noted above, I have also been engaged in a number of other studies related to the response of aerospace structures to high speed impact. These efforts have included an analysis of window materials impact data [55], a study of the effect of the location of an intervening MLI blanket within a dual-wall system on the impact response of the system [56], the use of corrugated bumpers instead of monolith bumpers [57], shock-physics-based modelling of hole formation in a thin plate [58], effect of pressure wall material on perforation response [59], the reliability of results obtained the simultaneously-launched multiple projectiles [60], and the design of penetration resistant lunar habitats [61-63].

12. Concluding Thoughts

In recent years I have been fortunate to have been asked to serve on several NRC/NAE and NESC Technical Committees. These committees have explored the resiliency of the Space Shuttle against MMOC impacts [64],

assessed NASA's BUMPER II computer code as its primary risk assessment tool [65], its overall MMOD program and program elements [66], and the U.S. Air Force's astrodynamics standards [67]. In other instances, these committees have wrestled with technical issue faced by existing and emerging NASA programs, such as Orion Crew Exploration Vehicle [68], the International Space Station [69,70], and the new JPSS satellite. In all instances, the committee were able to provide advice and technical assistance to NASA to help it meet is goals and objectives. Looking back, I would say that the road has been fun, interesting, and educational. I have been fortunate to work with many smart, talented people. I continuing to enjoy solving problems, and I hope to be able to continue working in this area with many more such individuals for many years ahead!

Acknowledgements

The author wishes to acknowledge the support provided by a wide variety of agencies, institutes, and corporations that made possible the studies noted previously, including NASA (MSFC, JSC, JPL, and NESC), NSF, AFOSR, ARL, ARO, Fraunhofer/EMI, the Humboldt Foundation, and Sandia National Laboratories.

References

[1] Whipple, F.L., "Meteorites and space travel", *Astronomical Journal*, Vol. 52, 1947, p. 137.
[2] Schonberg, W.P., "The Development of Ballistic Limit Equations for Dual-Wall Spacecraft Shielding: A Concise History and Suggestions for Future Development", 49th AIAA/ASME/ ASCE/AHS Structures, Structural Dynamics and Materials Conference, AIAA Paper No. 2008-1966, Chicago, IL, April, 2008.
[3] Schonberg, W.P., "Hypervelocity Impact Penetration Phenomena in Aluminum Space Structures", *Journal of Aerospace Engineering*, Vol. 3, No. 3, 1990, pp. 174-185.
[4] Schonberg, W.P., and Taylor, R.A., "Penetration and Ricochet Phenomena in Multi-Sheet Structures under Oblique Hypervelocity Impact", *AIAA Journal*, Vol. 27, 1989, pp. 639-646.
[5] Schonberg, W.P., "Characterizing Secondary Debris Impact Ejecta", *International Journal of Impact Engineering*, Vol. 26, 2001, pp. 713-724.
[6] Schonberg, W.P., and Taylor, R.A., "Exterior Spacecraft Subsystem Protective Shielding Analysis and Design", *Journal of Spacecraft and Rockets*, Vol. 27, No. 3, 1990, pp. 267-274.
[7] Schonberg, W.P., "Assessing the Resiliency of Composite Structural Systems and Materials Used in Earth-Orbiting Spacecraft to Hypervelocity Projectile Impact" *in* Predictive Modeling of Dynamic Processes, S. Hiermaier, *ed.*, Springer Verlag, 2009 (invited).
[8] Schonberg, W.P., "Protecting Earth-orbiting Spacecraft against Micro-Meteoroid/Orbital Debris Impact Damage Using Composite Structural Systems and Materials: An Overview", *Advances in Space Research*, Vol. 45, 2010, pp. 709-720.
[9] Schonberg, W.P., "Protecting Spacecraft Against Orbital Debris Impact Damage Using Composite Materials", *Composites Part A-Applied Science & Manufacturing*, Vol. 31, No. 8, 2000, pp. 869-878.
[10] Schonberg, W.P., Hypervelocity Impact Response of Honeycomb Sandwich Panels, Report No. A-04/08, Fraunhofer Ernst-Mach-Institute, Freiburg, Germany, January 2008.
[11] Schonberg WP (1990). "Hypervelocity Impact Response of Spaced Composite Material Structures", *International Journal of Impact Engineering*, 10:509-523.
[12] Christiansen, E.L., Evaluation of Space Station Meteoroid/Debris Shielding Materials. Report No. 87-163, Eagle Engineering, Inc, Houston, Texas, 1987.
[13] Schonberg, W.P., Walker, E.J., "Use of Composite Materials in Multi-Wall Structures to Prevent Perforation by Hypervelocity Projectiles", *Composite Structures*, Vol. 19, 1991, pp. 15-40.
[14] Schonberg, W.P., "Protecting Spacecraft against Meteoroid/Orbital Debris Impact Damage: An Overview", *Space Debris*, Vol. 1, 2001, pp. 195-210.
[15] Munjal, A.K., "Minimizing Hypervelocity Micrometeoroid Impact Damage to Composite Space Structures." Paper No. III.4, Proceedings of the 1998 Leonid Meteoroid Storm and Satellite Threat Conference, The Aerospace Corporation, Los Angeles, California, 1998.
[16] Christiansen, E.L., Kerr, J.H., "Projectile Shape Effects on Shielding Performance at 7 km/s and 11 km/s." *International Journal of Impact Engineering*, Vol. 20, 1997, pp. 165-172.
[17] Schonberg, W.P., Walker, E.J., "Hypervelocity Impact of Dual-Wall Structures with Graphite/Epoxy Inner Walls", *Composites Engineering*, Vol. 4, No. 10, 1994, pp. 1045-1054.
[18] Schäfer, F., Ryan, S., et al, "Ballistic Limit Equation for Equipment Placed Behind Satellite Structure Walls", *International Journal of Impact Engineering*, Vol. 35, 2008, pp. 1784-1791.
[19] Ryan, S., Schäfer, F., et al, "A Ballistic Limit Equation for Hypervelocity Impacts on Composite Honeycomb Sandwich Panel Satellite Structures", *Advances in Space Research,* Vol. 41, No. 7, 2007, pp. 1152-1166.
[20] Schonberg, W.P., Schaefer, F., and Putzar, R., "Predicting the Perforation Response of Honeycomb Sandwich Panels Using Ballistic Limit Equations," *Journal of Spacecraft and Rockets*, Vol. 46, No. 5, 2009, pp. 976-981.
[21] Schonberg, W.P., Schaefer, F., and Putzar, R., "Hypervelocity Impact Response of Honeycomb Sandwich Panels", *Acta Astronautica*, Vol. 66, 2010, pp. 455-466.
[22] Schonberg, W.P., and Darzi, K., "Effect of Projectile Shape and Material on the Hypervelocity Impact Response of Aluminum Dual-Wall Structures", *Journal of Aerospace Engineering*, Vol. 5, No. 4, 1992, pp. 405-424.
[23] Morrison, R.H., Investigation of Projectile Shape Effects in Hypervelocity Impact of a Double-Sheet Structure, NASA TN D-6944,

Washington, D.C., 1972.
[24] Piekutowski, A.J., "Hypervelocity impact of non-spherical projectiles: observations and lessons learned from impact tests", in: Fair H, ed, Proceedings of the Hypervelocity Shielding Workshop, Institute of Advanced Technology, Texas, March 1998.
[25] Schonberg, W.P., and Peck, J.A., "Parametric Investigation of Multi-Wall Structural Response to Hypervelocity Cylindrical Projectile Impact", *Computers and Structures*, Vol. 49, No. 4, 1993, pp. 719-746.
[26] Hu, K., and Schonberg, W.P., "Ballistic Limit Curves for Non-Spherical Projectiles Impacting Dual-Wall Systems", *International Journal of Impact Engineering*, Vol. 29, 2003, pp. 345-356.
[27] Schonberg, W.P, and Williamsen, J.E., "RCS-Based Ballistic Limit Curves for Non-Spherical Projectiles Impacting Dual-Wall Spacecraft Systems", *International Journal of Impact Engineering*, Vol. 33, 2006, pp. 763-770.
[28] Williamsen, J.E., Schonberg, W.P., Evans, H., and Evans, S., "A Comparison of NASA, DoD, and Hydrocode Spherical and Non-spherical Ballistic Limit Predictions for Dual-Wall Targets and Their Effect on Spacecraft Risk", *International Journal of Impact Engineering*, Vol. 35, 2008, pp. 1870-1877.
[29] Williamsen, J.E., Schonberg, W.P., and Jenkin, A.B., "On the Effect of Considering More Realistic Particle Shape and Mass Parameters in MMOD Risk Assessments", *Advances in Space Research*, Vol. 47, 2011, pp. 1006–1019.
[30] Celestian, J.P., and Schonberg, W.P., "Dynamic Response of the Space Station Freedom to a Module Perforation by a Hypervelocity Impact", *International Journal of Impact Engineering*, Vol. 13, No. 2, 1993, pp. 353-365.
[31] Gehring, J. W., Lathrop, B. L., and Warnica, R. L., Spacecraft Interior Hazards from Hypervelocity Impact, GM Defense Research Laboratory, TR-66-13, Santa Barbara, CA, March 1966.
[32] Long, L.L., and Hammitt, R.L., "Meteoroid Perforation Effects on Space Cabin Design," AIAA Paper 69-365, April 1969.
[33] Schonberg, W.P., Serrano, J., and Williamsen, J.E., "An Internal Effects Model for a Habitable Spacecraft Module Perforated by an Orbital Debris Particle", *Journal of Spacecraft and Rockets*, Vol. 34, No. 3, 1997, pp. 325-333.
[34] Schonberg, W.P., and Williamsen, J.E., "Cracking Characteristics of Dual-Wall Structures Following Simulated Orbital Debris Particle Impact", *Journal of Spacecraft and Rockets*, Vol. 34, No. 3, 1997, pp. 318-324.
[35] Schonberg, W.P., and Williamsen, J.E., "Empirical Hole Size and Crack Length Models for Dual-Wall Systems under Hypervelocity Projectile Impact", *International Journal of Impact Engineering*, Vol. 20, 1997, pp. 711-722.
[36] Williamsen, J.E., Evans, H.A., and Schonberg, W.P., "Effect of Multi-Wall System Composition on Survivability for Spacecraft Impacted by Orbital Debris", *Space Debris*, Vol. 1, No. 1, 1999, pp. 37-43.
[37] Schonberg, W.P., "Onset of Petaling in a Thin Spacecraft Wall Perforated by an Orbital Debris Particle", *Proceedings of the Institution of Mechanical Engineers, Part G (Journal of Aerospace Engineering)*, Vol. 212, 1998, pp. 407-414.
[38] Schonberg, W.P. and Mohamed, E., "Analytical Hole Size and Crack Length Models for Multi-Wall Systems under Hypervelocity Projectile Impact", *International Journal of Impact Engineering*, Vol. 23, 1999, pp. 835-846.
[39] Schonberg, W.P., "Hole Size and Crack Length Models for Spacecraft Walls under Oblique Hypervelocity Projectile Impact", *Aerospace Science and Technology*, Vol. 3, 1999, pp. 461-471.
[40] Williamsen, J.E., Schonberg, W.P., and Evans, H.J., "Generic Module Wall Damage Prediction Equations for Habitable Spacecraft Crew Survivability Evaluations", *International Journal of Impact Engineering*, Vol. 56, 2013, pp 71-81.
[41] Schonberg, W.P., and Cooper, D., "Repeatability and Uncertainty Analysis of NASA/MSFC Light Gas Gun Test Data", *AIAA Journal*, Vol. 32, No. 5, 1994, pp. 1058-1065.
[42] Schonberg, W.P., Evans, H.J, Williamsen, J.E., Boyer, R.L., and Nakayama, G.S., "Uncertainty Considerations for Ballistic Limit Equations for Aerospace Structural Systems", Proceedings of the ASME International Mechanical Engineering Congress and Exposition, Paper No. IMECE-2005-79709, Orlando, Florida, November, 2005.
[43] Schonberg, W.P., Evans, H.J, Williamsen, J.E., Boyer, R.L., and Nakayama, G.S., "Uncertainty Considerations for Ballistic Limit Equations", Proceedings of the 4th European Conference on Space Debris, Darmstadt, Germany, April, 2005.
[44] Schonberg, W.P., "Debris Cloud Material Characterization for Hypervelocity Impacts of Single- and Multi-Material Projectiles on Thin Target Plates", *Shock and Vibration*, Vol. 2, No. 4, 1995, pp. 273-287.
[45] Depczuk, D. and Schonberg, W.P., "Characterizing the Debris Clouds Created in an Oblique Orbital Debris Particle Impact", *Journal of Aerospace Engineering*, Vol. 16, No. 4, pp. 177-190, 2003.
[46] Schonberg, W.P., and Yang, F., "Predicting the Response of Space Structures to Orbital Debris Particle Impact", *International Journal of Impact Engineering*, Vol. 14, 1993, pp. 647-658.
[47] Schonberg, W.P. and Ebrahim, A., "Modelling Oblique Hypervelocity Impact Phenomena Using Elementary Shock Physics", *International Journal of Impact Engineering*, Vol. 23, 1999, pp. 823-834.
[48] Schonberg, W.P., MMOD Impact of Pressurized Tanks: Initial Data Analyses and First-Principles-Based Calculations, Report No. JPL-D-93584, Jet Propulsion Laboratory, Pasadena, California, August, 2014.
[59] Schonberg, W.P., "Effect of Internal Stress Fields on the Perforation Response of Dual-Wall Structures under Hypervelocity Impact", *International Journal of Impact Engineering*, Vol. 14, 1993, pp. 637-646.
[50] Christiansen, E.L., "Design and Performance Equations for Advanced Meteoroid and Debris Shields", *International Journal of Impact Engineering*, Vol. 14, 1993, pp. 145-156.
[51] Christiansen, E.L., and J.H. Kerr, "Ballistic Limit Equations for Spacecraft Shielding", *International Journal of Impact Engineering*, Vol. 26, 2001, pp. 93-104.
[52] Schonberg, W.P., and Ratliff, J.M., "A First-Principles-Based Model for Crack Formation in a Pressurized Tank Following an MMOD Impact", Proceedings of the 2015 Hypervelocity Impact Symposium, Boulder, CO, April, 2015; in *Procedia Engineering* (to appear).
[53] Nahra, H.K., et al, "Hypervelocity Impact of Unstressed and Stressed Titanium in a Whipple Configuration in Support of the Orion Crew Exploration Vehicle Service Module Propellant Tanks", Proceedings of the 2010 Hypervelocity Impact Symposium, F. Schaefer and S. Hiermeier, *eds*, Ernst Mach Institute, Freiburg, Germany, April 1010 (also NASA TM-2010-216804).
[54] Nahra, H.K., et al, "Burst Pressure Failure of Titanium Tanks Damaged by Secondary Plumes From Hypervelocity Impacts on Aluminum Shields", Proceedings of the 2011 Shock Compression of Condensed Matter Conference, Chicago, Illinois, American Institute of Physics, New York, 2012, pp. 100-103.

[55] Schonberg, W.P., "Hypervelocity Projectile Impact of Spacecraft Windows", *Journal of Spacecraft and Rockets*, Vol. 28, No. 1, 1991, pp. 118-123.
[56] Schonberg, W.P., "Effect of Multi-Layer Insulation Thickness and Location on the Hypervelocity Impact Response of Dual-Wall Structures", *Acta Astronautica*, Vol. 32, No. 9, 1994, pp. 577-589.
[57] Schonberg, W.P., and Tullos, R., "Spacecraft Wall Design for Increased Protection against Penetration by Space Debris Impacts", *AIAA Journal*, Vol. 29, No. 12, 1991, pp. 2207-2214.
[58] Jolly, W.H., and Schonberg, W.P., "Analytical Prediction of Hole Size Due to Hypervelocity Impact of Spherical Projectiles", *Shock and Vibration*, Vol. 4., Nos. 5-6, 1997, pp. 379-390.
[59] Schonberg, W.P., "Aluminum 2219-T87 and 5456-H116: A Comparative Study of Pressure Wall Materials in Dual-Wall Structures Under Hypervelocity Impact", *Acta Astronautica*, Vol. 26, No. 11, 1992, pp. 799-812.
[60] Schonberg, W.P., Evans, S., and Bjorkman, M.D., "Hypervelocity Impact Testing of Multi-Wall Targets Using Multiple Simultaneously Launched Projectiles", *Journal of Spacecraft and Rockets*, Vol. 50, No. 2, 2013, pp. 358-364.
[61] Schonberg, W.P., Sustainable Lunar Habitat Protection Against Damage by Meteoroid Impacts, Report No. A-03/08, Fraunhofer Ernst-Mach-Institute, Freiburg, Germany, January 2008.
[62] Schonberg, W.P., Putzar, R., and Schaefer, F., "Lunar Habitat Protection against Meteoroid Impact Damage", *in* Lunar Settlements, H. Benaroya, *ed.*, CRC Press, 2010.
[63] Schonberg, W.P., Schaefer, F., and Putzar, R., "Some Comments on the Protection of Lunar Habitats Against Damage from Meteoroid Impacts", *ASCE Journal of Aerospace Engineering*, Vol. 23, No. 1, 2010, pp. 90-97.
[64] National Research Council, Protecting the Space Shuttle from Meteoroids and Orbital Debris, National Academy Press, Washington, DC, 1997.
[65] NASA Engineering Safety Center (NESC), Independent Technical Inspection of the Bumper-II Micrometeoroid and Orbital Debris Risk Assessment, NASA Engineering and Safety Center, Report No. RP-05-66, April, 2005.
[66] National Research Council, Limiting Future Collision Risk to Spacecraft: An Assessment of NASA's Meteoroid and Orbital Debris Programs, National Academy Press, Washington, DC, 2011.
[67] National Research Council, Continuing Kepler's Quest: Assessing Air Force Space Command's Astrodynamics Standards, National Academy Press, Washington, DC, 2012.
[68] NASA Engineering Safety Center (NESC), Independent Review of Constellation (Cx) Orion Vehicle Micrometeoroids and Orbital Debris (MMOD) Risk Analysis, NASA Engineering and Safety Center, Report No. NESC-RP-08-00468, January, 2009.
[69] NASA Engineering Safety Center (NESC), Independent Review of United States and Russian Probabilistic Risk Assessments (PRAs) for the International Space Station (ISS) Mini Research Module #2 (MRM-2) Micrometeoroid and Orbital Debris (MMOD) Risk, NASA Engineering and Safety Center, Report No. NESC-RP-09-00592, February, 2011.
[70] NASA Engineering Safety Center (NESC), Lightweight Installable Micrometeoroid and Orbital Debris (MMOD) Shield Concepts for International Space Station (ISS) Modules, NASA Engineering and Safety Center, Report No. NESC-RP- 09-00593, January, 2011 (also NASA TM-2011-217044, March, 2011).